Author(s): Langer, Ulrich; Repin, Sergey; Wolfmayr, Monika

Title: Functional a posteriori Error Estimates for Time-periodic Parabolic Optimal Control Problems

Year: 2016

Version:

Please cite the original version:

Langer, U., Repin, S., & Wolfmayr, M. (2016). Functional a posteriori Error Estimates for Time-periodic Parabolic Optimal Control Problems. Numerical Functional Analysis and Optimization, 37(10), 1267-1294. https://doi.org/10.1080/01630563.2016.1200077

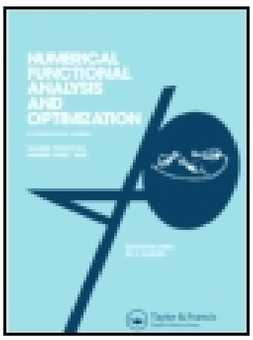

Taylor & Francis
Taylor & Francis Group

Numerical Functional Analysis and Optimization

ISSN: 0163-0563 (Print) 1532-2467 (Online) Journal homepage: http://www.tandfonline.com/loi/lnfa20

Functional a posteriori Error Estimates for Time-periodic Parabolic Optimal Control Problems

Ulrich Langer, Sergey Repin & Monika Wolfmayr

To cite this article: Ulrich Langer, Sergey Repin & Monika Wolfmayr (2016): Functional a posteriori Error Estimates for Time-periodic Parabolic Optimal Control Problems, Numerical Functional Analysis and Optimization, DOI: 10.1080/01630563.2016.1200077

To link to this article: http://dx.doi.org/10.1080/01630563.2016.1200077

Accepted author version posted online: 03 Aug 2016.
Published online: 03 Aug 2016.

Functional a Posteriori Error Estimates for Time-periodic Parabolic Optimal Control Problems

Ulrich Langer[1], Sergey Repin[2], and Monika Wolfmayr[3]

[1]Institute of Computational Mathematics, Johannes Kepler University Linz, Linz, Austria

[2]V. A. Steklov Institute of Mathematics in St. Petersburg, St. Petersburg, Russia, and University of Jyväskylä, Finland

[3]Johann Radon Institute for Computational and Applied Mathematics, Linz, Austria

Abstract

This paper is devoted to the *a posteriori* error analysis of multiharmonic finite element approximations to distributed optimal control problems with time-periodic state equations of parabolic type. We derive *a posteriori* estimates of functional type, which are easily computable and provide guaranteed upper bounds for the state and co-state errors as well as for the cost functional. These theoretical results are confirmed by several numerical tests that show high efficiency of the *a posteriori* error bounds.

Received 23 November 2015; Revised 6 June 2016; Accepted 7 June 2016.

Monika Wolfmayr, Johann Radon Institute for Computational and Applied Mathematics, Altenbergerstraße 69, 4040 Linz, Austria; E-mail: monika.wolfmayr@ricam.oeaw.ac.at

1. INTRODUCTION

We consider optimal control problems with time-periodic parabolic state equations. Problems of this type often arise in different practical applications, e.g., in electromagnetics, chemistry, biology, or heat transfer, see also (1; 2; 3). Moreover, optimal control problems are the subject matter of lots of different works, see, e.g., (4; 5; 6; 7) and the references therein. The multiharmonic finite element method (MhFEM) is well adapted to the class of parabolic time-periodic problems. Within the framework of this method, the state functions are expanded into Fourier series in time with coefficients depending on the spatial variables. In numerical computations, these series are truncated and the Fourier coefficients are approximated by the finite element method (FEM). This scheme leads to the MhFEM (also called harmonic-balanced FEM), which was successfully used for the simulation of electromagnetic devices described by nonlinear eddy current problems with harmonic excitations, see, e.g., (8; 9; 10; 11; 12) and the references therein. Later, the MhFEM has been applied to linear time-periodic parabolic boundary value and optimal control problems (13; 14; 15; 16; 17) and to linear time-periodic eddy current problems and the corresponding optimal control problems (18; 19; 20). In the MhFEM setting, we are able to establish inf-sup and sup-sup conditions, which provide existence and uniqueness of the solution to parabolic time-periodic problems. For linear time-periodic parabolic problems, MhFEM is a natural and very efficient numerical technology based on the decoupling of computations related to different modes.

There are only a few publications, where *a posteriori* error estimates of the functional type were derived for optimal control problems with PDE-constraints (for the concerned problems with elliptic state equations see (21) and the references therein). This paper is aimed to make a step towards the creation of fully reliable error estimation methods for distributed time-periodic parabolic optimal control problems. We consider the multiharmonic finite element (MhFE) approximations of the reduced optimality system, and derive guaranteed and fully computable bounds for the discretization errors. For this purpose, we use the functional *a posteriori* error estimation techniques earlier introduced by S. Repin, see, e.g., the papers on parabolic problems (22; 23) as well as on optimal control problems (24; 25), the books (21; 26) and the references therein. In particular, our functional *a posteriori* error analysis uses the techniques close to those suggested in (22), but the analysis contains essential changes due to the MhFEM setting. In (27), the authors already derived functional *a posteriori* error estimates for MhFE approximations to parabolic time-periodic boundary value problems. In this work, essentially new results have been obtained for the MhFE approximations to state and co-state, which are the unique solutions of the reduced optimality system. It is worth mentioning that these *a posteriori* error estimates for the state and co-state immediately yield the corresponding *a posteriori* error estimates for the control. In addition to these results, we deduce fully computable estimates from above of the cost functional. In fact, we generate a new formulation of the optimal control problem, in which (unlike the original statement) the state equations are accounted in terms of penalties. It is proved that the modified cost functional attains its infimum at the optimal control and the respective state function.

Therefore, in principle, we can use it as an object of direct minimization, which value on each step provides a guaranteed upper bound of the cost functional. We want to mention here that computable and realistic estimates from below of the cost functional are also important. In some cases we can deduce them (see (21) or (28)). We think that this is also possible to do for the considered class of problems. However, a systematic consideration of this question needs a considerable space and is planned for a subsequent publication.

The paper is organized as follows: In Section 2, we discuss the time-periodic parabolic optimal control problem and the corresponding optimality system. The multiharmonic finite element discretization of this space-time weak formulation is considered in Section 3. Section 4 is devoted to the derivation of functional *a posteriori* error estimates for the optimality system associated with the multiharmonic setting. In Section 5, we present new results related to guaranteed and computable bounds of the cost functional. In the final Section 6, we discuss some implementation issues and present the first numerical results.

2. A TIME-PERIODIC PARABOLIC OPTIMAL CONTROL PROBLEM

Let $Q_T := \Omega \times (0, T)$ denote the space-time cylinder and $\Sigma_T := \Gamma \times (0, T)$ its mantle boundary, where the spatial domain $\Omega \subset \mathbb{R}^d$, $d = \{1, 2, 3\}$, is assumed to be a bounded Lipschitz domain with boundary $\Gamma := \partial\Omega$, and $(0, T)$ is a given time interval. Let $\lambda > 0$

be the regularization or cost parameter. We consider the following parabolic time-periodic optimal control problem:

$$\min_{y,u} \mathcal{J}(y, u) := \frac{1}{2} \int_0^T \int_\Omega (y(\boldsymbol{x}, t) - y_d(\boldsymbol{x}, t))^2 \, d\boldsymbol{x} \, dt + \frac{\lambda}{2} \int_0^T \int_\Omega (u(\boldsymbol{x}, t))^2 \, d\boldsymbol{x} \, dt \tag{1}$$

subject to the parabolic time-periodic boundary value problem

$$\left.\begin{array}{ll} \sigma(\boldsymbol{x}) \, \partial_t y(\boldsymbol{x}, t) - \operatorname{div}(v(\boldsymbol{x}) \nabla y(\boldsymbol{x}, t)) = u(\boldsymbol{x}, t) & (\boldsymbol{x}, t) \in Q_T, \\ y(\boldsymbol{x}, t) = 0 & (\boldsymbol{x}, t) \in \Sigma_T, \\ y(\boldsymbol{x}, 0) = y(\boldsymbol{x}, T) & \boldsymbol{x} \in \overline{\Omega}. \end{array}\right\} \tag{2}$$

Here, y and u are the state and control functions, respectively. The coefficients $\sigma(\cdot)$ and $v(\cdot)$ are uniformly bounded and satisfy the conditions

$$0 < \underline{\sigma} \le \sigma(\boldsymbol{x}) \le \overline{\sigma}, \quad \text{and} \quad 0 < \underline{v} \le v(\boldsymbol{x}) \le \overline{v}, \quad \boldsymbol{x} \in \Omega, \tag{3}$$

where $\underline{\sigma}$, $\overline{\sigma}$, $\underline{v}$ and $\overline{v}$ are positive constants. As usual, the cost functional (1) contains a penalty term weighted with a positive factor λ. This term restricts (in the integral sense) values of the control function u.

We can reformulate the problem (1)–(2) in an equivalent form. For this purpose, we introduce the formal Lagrangian

$$\mathcal{L}(y, u, p) := \mathcal{J}(y, u) - \int_0^T \int_\Omega \big(\sigma \partial_t y - \operatorname{div}(v \nabla y) - u\big) p \, d\boldsymbol{x} \, dt, \tag{4}$$

which has a saddle point, see, e.g., (5; 6) and the references therein. The proper sets for which this saddle point problem is correctly stated are defined later. Since the saddle point exists, the corresponding solutions satisfy the system of necessary conditions

$$\mathscr{L}_p(y, u, p) = 0, \quad \mathscr{L}_y(y, u, p) = 0, \quad \mathscr{L}_u(y, u, p) = 0. \tag{5}$$

Using the second condition, we can eliminate the control u from the optimality system (5), i.e.,

$$u = -\lambda^{-1} p \quad \text{in } Q_T. \tag{6}$$

From (6) it appears very natural to choose u and p from the same space. Moreover, we arrive at a reduced optimality system, written in its classical formulation as

$$\left.\begin{array}{ll} \sigma(\boldsymbol{x})\, \partial_t y(\boldsymbol{x}, t) - \operatorname{div}(v(\boldsymbol{x}) \nabla y(\boldsymbol{x}, t)) = -\lambda^{-1} p(\boldsymbol{x}, t) & (\boldsymbol{x}, t) \in Q_T, \\ y(\boldsymbol{x}, t) = 0 & (\boldsymbol{x}, t) \in \Sigma_T, \\ y(\boldsymbol{x}, 0) = y(\boldsymbol{x}, T) & \boldsymbol{x} \in \overline{\Omega}, \\ -\sigma(\boldsymbol{x})\, \partial_t p(\boldsymbol{x}, t) - \operatorname{div}(v(\boldsymbol{x}) \nabla p(\boldsymbol{x}, t)) = y(\boldsymbol{x}, t) - y_d(\boldsymbol{x}, t) & (\boldsymbol{x}, t) \in Q_T, \\ p(\boldsymbol{x}, t) = 0 & (\boldsymbol{x}, t) \in \Sigma_T, \\ p(\boldsymbol{x}, T) = p(\boldsymbol{x}, 0) & \boldsymbol{x} \in \overline{\Omega}. \end{array}\right\} \tag{7}$$

In order to determine weak (generalized) solutions of (7), we define the following spaces (here and later on, the notation is similar to that was used in (29; 30)):

$$H^{1,0}(Q_T) = \{v \in L^2(Q_T) : \nabla v \in [L^2(Q_T)]^d\},$$

$$H^{0,1}(Q_T) = \{v \in L^2(Q_T) : \partial_t v \in L^2(Q_T)\},$$

$$H^{1,1}(Q_T) = \{v \in L^2(Q_T) : \nabla v \in [L^2(Q_T)]^d, \partial_t v \in L^2(Q_T)\},$$

which are endowed with the norms

$$\|v\|_{1,0} := \left(\int_{Q_T} \left(v(\boldsymbol{x}, t)^2 + |\nabla v(\boldsymbol{x}, t)|^2 \right) \, d\boldsymbol{x} \, dt \right)^{1/2},$$

$$\|v\|_{0,1} := \left(\int_{Q_T} \left(v(\boldsymbol{x}, t)^2 + |\partial_t v(\boldsymbol{x}, t)|^2 \right) \, d\boldsymbol{x} \, dt \right)^{1/2},$$

$$\|v\|_{1,1} := \left(\int_{Q_T} \left(v(\boldsymbol{x}, t)^2 + |\nabla v(\boldsymbol{x}, t)|^2 + |\partial_t v(\boldsymbol{x}, t)|^2 \right) \, d\boldsymbol{x} \, dt \right)^{1/2},$$

respectively. Here, $\nabla = \nabla_{\boldsymbol{x}}$ is the spatial gradient and ∂_t denotes the weak derivative with respect to time. Also we define subspaces of the above introduced spaces by putting subindex zero if the functions satisfy the homogeneous Dirichlet condition on Σ_T and subindex *per* if they satisfy the time-periodical condition $v(\boldsymbol{x}, 0) = v(\boldsymbol{x}, T)$. All inner products and norms in L^2 related to the whole space-time domain Q_T are denoted by $\langle \cdot, \cdot \rangle$ and $\| \cdot \|$, respectively. If they are associated with the spatial domain Ω, then we write $\langle \cdot, \cdot \rangle_\Omega$ and $\| \cdot \|_\Omega$. The symbols $\langle \cdot, \cdot \rangle_{1,\Omega}$ and $\| \cdot \|_{1,\Omega}$ denote the standard inner products and norms of the space $H^1(\Omega)$.

The functions used in our analysis are presented in terms of Fourier series, e.g., the Fourier representation of the function $v(\boldsymbol{x}, t)$ is given by the series

$$v(\boldsymbol{x}, t) = v_0^c(\boldsymbol{x}) + \sum_{k=1}^{\infty} \left(v_k^c(\boldsymbol{x}) \cos(k\omega t) + v_k^s(\boldsymbol{x}) \sin(k\omega t) \right), \tag{8}$$

where

$$v_0^c(\boldsymbol{x}) = \frac{1}{T} \int_0^T v(\boldsymbol{x}, t) \, dt,$$

$$v_k^c(\boldsymbol{x}) = \frac{2}{T} \int_0^T v(\boldsymbol{x}, t) \cos(k\omega t) \, dt, \quad \text{and} \quad v_k^s(\boldsymbol{x}) = \frac{2}{T} \int_0^T v(\boldsymbol{x}, t) \sin(k\omega t) \, dt$$

are the Fourier coefficients, T denotes the period, and $\omega = 2\pi/T$ is the frequency. Since the problem has time-periodical conditions, these representations of the exact solution and respective approximations are quite natural. In what follows, we also use the spaces

$$H^{0,\frac{1}{2}}_{per}(Q_T) = \{v \in L^2(Q_T) : \left\|\partial_t^{1/2} v\right\| < \infty\},$$

$$H^{1,\frac{1}{2}}_{per}(Q_T) = \{v \in H^{1,0}(Q_T) : \left\|\partial_t^{1/2} v\right\| < \infty\},$$

$$H^{1,\frac{1}{2}}_{0,per}(Q_T) = \{v \in H^{1,\frac{1}{2}}_{per}(Q_T) : v = 0 \text{ on } \Sigma_T\},$$

where $\left\|\partial_t^{1/2} v\right\|$ is defined in the Fourier space by the relation

$$\left\|\partial_t^{1/2} v\right\|^2 := |v|^2_{0,\frac{1}{2}} := \frac{T}{2}\sum_{k=1}^{\infty} k\omega \|\boldsymbol{v}_k\|^2_\Omega. \tag{9}$$

Here, $\boldsymbol{v}_k = (v_k^c, v_k^s)^T$ for all $k \in \mathbb{N}$, see also (16). These spaces can be considered as Hilbert spaces if we introduce the following (equivalent) products:

$$\langle \partial_t^{1/2} y, \partial_t^{1/2} v\rangle := \frac{T}{2}\sum_{k=1}^{\infty} k\omega \langle \boldsymbol{y}_k, \boldsymbol{v}_k\rangle_\Omega, \quad \langle \sigma\partial_t^{1/2} y, \partial_t^{1/2} v\rangle := \frac{T}{2}\sum_{k=1}^{\infty} k\omega \langle \sigma\boldsymbol{y}_k, \boldsymbol{v}_k\rangle_\Omega.$$

The above introduced spaces allow us to operate with a "symmetrized" formulation of the problem (7) presented by (15). The seminorm and the norm of the space $H^{1,\frac{1}{2}}_{per}(Q_T)$ are defined by the relations

$$|v|^2_{1,\frac{1}{2}} := \|\nabla v\|^2 + \|\partial_t^{1/2} v\|^2 = T\,\|\nabla y_0^c\|^2_\Omega + \frac{T}{2}\sum_{k=1}^{\infty}\left(k\omega\|\boldsymbol{v}_k\|^2_\Omega + \|\nabla \boldsymbol{v}_k\|^2_\Omega\right) \quad \text{and}$$

$$\|v\|^2_{1,\frac{1}{2}} := \|v\|^2 + |v|^2_{1,\frac{1}{2}} = T\left(\|y_0^c\|^2_\Omega + \|\nabla y_0^c\|^2_\Omega\right) + \frac{T}{2}\sum_{k=1}^{\infty}\left((1+k\omega)\|\boldsymbol{v}_k\|^2_\Omega + \|\nabla \boldsymbol{v}_k\|^2_\Omega\right),$$

respectively. Using Fourier type series, it is easy to define the function "orthogonal" to v:

$$v^{\perp}(\boldsymbol{x}, t) := \sum_{k=1}^{\infty} \left(-v_k^c(\boldsymbol{x}) \sin(k\omega t) + v_k^s(\boldsymbol{x}) \cos(k\omega t)\right)$$
$$= \sum_{k=1}^{\infty} \underbrace{(v_k^s(\boldsymbol{x}), -v_k^c(\boldsymbol{x}))}_{=:(-\boldsymbol{v}_k^{\perp})^T} \cdot \begin{pmatrix} \cos(k\omega t) \\ \sin(k\omega t) \end{pmatrix}.$$

Obviously, $\|\boldsymbol{u}_k^{\perp}\|_{\Omega} = \|\boldsymbol{u}_k\|_{\Omega}$ and we find that

$$\left\|\partial_t^{1/2} v^{\perp}\right\|^2 = \frac{T}{2} \sum_{k=1}^{\infty} k\omega \|\boldsymbol{v}_k^{\perp}\|_{\Omega}^2 = \frac{T}{2} \sum_{k=1}^{\infty} k\omega \|\boldsymbol{v}_k\|_{\Omega}^2 = \left\|\partial_t^{1/2} v\right\|^2 \quad \forall\, v \in H_{per}^{0,\frac{1}{2}}(Q_T).$$

Henceforth, we use the following subsidiary result (which proof can be found in (27)):

Lemma 1. *The identities*

$$\langle \sigma \partial_t^{1/2} y, \partial_t^{1/2} v \rangle = \langle \sigma \partial_t y, v^{\perp} \rangle \quad \textit{and} \quad \langle \sigma \partial_t^{1/2} y, \partial_t^{1/2} v^{\perp} \rangle = \langle \sigma \partial_t y, v \rangle \tag{10}$$

are valid for all $y \in H_{per}^{0,1}(Q_T)$ *and* $v \in H_{per}^{0,\frac{1}{2}}(Q_T)$.

Also, we recall the orthogonality relations (see (16; 17))

$$\left.\begin{aligned} &\langle \sigma \partial_t y, y \rangle = 0 \qquad \text{and } \langle \sigma y^{\perp}, y \rangle = 0 \quad \forall\, y \in H_{per}^{0,1}(Q_T), \\ &\langle \sigma \partial_t^{1/2} y, \partial_t^{1/2} y^{\perp} \rangle = 0 \text{ and } \langle v \nabla y, \nabla y^{\perp} \rangle = 0 \;\forall\, y \in H_{per}^{1,\frac{1}{2}}(Q_T), \end{aligned}\right\} \tag{11}$$

and the identity

$$\int_{Q_T} \xi\, \partial_t^{1/2} v^{\perp}\, d\boldsymbol{x}\, dt = -\int_{Q_T} \partial_t^{1/2} \xi^{\perp}\, v\, d\boldsymbol{x}\, dt \quad \forall\, \xi, v \in H_{per}^{0,\frac{1}{2}}(Q_T), \tag{12}$$

which should again be understood in the sense of Fourier series. **Similarly, we define**

$$\langle \xi, \partial_t^{1/2} v \rangle := \frac{T}{2} \sum_{k=1}^{\infty} (k\omega)^{1/2} \langle \boldsymbol{\xi}_k, \boldsymbol{v}_k \rangle_\Omega. \tag{13}$$

We note that for functions presented in terms of Fourier series the standard Friedrichs inequality holds in Q_T. Indeed,

$$\begin{aligned} \|\nabla u\|^2 &= \int_{Q_T} |\nabla u|^2 \, d\boldsymbol{x}\, dt = T \, \|\nabla u_0^c\|_\Omega^2 + \frac{T}{2} \sum_{k=1}^{\infty} \|\nabla \boldsymbol{u}_k\|_\Omega^2 \\ &\geq \frac{1}{C_F^2} \left(T \, \|u_0^c\|_\Omega^2 + \frac{T}{2} \sum_{k=1}^{\infty} \|\boldsymbol{u}_k\|_\Omega^2 \right) = \frac{1}{C_F^2} \|u\|^2. \end{aligned} \tag{14}$$

In order to derive the weak formulations of the equations (7), we multiply them by test functions $z, q \in H_{0,per}^{1,\frac{1}{2}}(Q_T)$, integrate over Q_T, and apply integration by parts with respect to the spatial variables and time using the second equation of (10). We arrive at the following "symmetric" space-time weak formulations of the reduced optimality system (7): Given the desired state $y_d \in L^2(Q_T)$, find y and p from $H_{0,per}^{1,\frac{1}{2}}(Q_T)$ such that

$$\left.\begin{aligned} \int_{Q_T} \left(y\, z - \nu(\boldsymbol{x}) \nabla p \cdot \nabla z + \sigma(\boldsymbol{x}) \partial_t^{1/2} p \, \partial_t^{1/2} z^\perp \right) d\boldsymbol{x}\, dt &= \int_{Q_T} y_d \, z \, d\boldsymbol{x}\, dt, \\ \int_{Q_T} \left(\nu(\boldsymbol{x}) \nabla y \cdot \nabla q + \sigma(\boldsymbol{x}) \partial_t^{1/2} y \, \partial_t^{1/2} q^\perp + \lambda^{-1} p\, q \right) d\boldsymbol{x}\, dt &= 0, \end{aligned}\right\} \tag{15}$$

for all test functions $z, q \in H_{0,per}^{1,\frac{1}{2}}(Q_T)$. We can represent (15) in a somewhat different form. For this purpose, it is convenient to introduce the bilinear form

$$\begin{aligned} \mathscr{B}((y,p),(z,q)) = \int_{Q_T} \Big(& y\, z - \nu(\boldsymbol{x}) \nabla p \cdot \nabla z + \sigma(\boldsymbol{x}) \partial_t^{1/2} p \, \partial_t^{1/2} z^\perp \\ & + \nu(\boldsymbol{x}) \nabla y \cdot \nabla q + \sigma(\boldsymbol{x}) \partial_t^{1/2} y \, \partial_t^{1/2} q^\perp + \lambda^{-1} p\, q \Big) \, d\boldsymbol{x}\, dt. \end{aligned} \tag{16}$$

Then (15) reads as

$$\mathcal{B}((y, p), (z, q)) = \langle (y_d, 0), (z, q) \rangle \quad \forall\, (z, q) \in (H^{1,\frac{1}{2}}_{0,per}(Q_T))^2.$$

3. MULTIHARMONIC FINITE ELEMENT APPROXIMATION

In order to solve the optimal control problem (1)–(2) approximately, we discretize the optimality system (15) by the MhFEM (see (16)). Using the Fourier series ansatz (8) in (15) and exploiting the orthogonality of $\cos(k\omega t)$ and $\sin(k\omega t)$, we arrive at the following problem: Find $\boldsymbol{y}_k, \boldsymbol{p}_k \in \mathbb{V} := V \times V = (H^1_0(\Omega))^2$ such that

$$\left.\begin{aligned} &\int_\Omega \left(\boldsymbol{y}_k \cdot \boldsymbol{z}_k - \nu(\boldsymbol{x})\nabla \boldsymbol{p}_k \cdot \nabla \boldsymbol{z}_k + k\omega\, \sigma(\boldsymbol{x}) \boldsymbol{p}_k \cdot \boldsymbol{z}_k^\perp\right) d\boldsymbol{x} = \int_\Omega \boldsymbol{y}_{dk} \cdot \boldsymbol{z}_k\, d\boldsymbol{x}, \\ &\int_\Omega \left(\nu(\boldsymbol{x})\nabla \boldsymbol{y}_k \cdot \nabla \boldsymbol{q}_k + k\omega\, \sigma(\boldsymbol{x}) \boldsymbol{y}_k \cdot \boldsymbol{q}_k^\perp + \lambda^{-1} \boldsymbol{p}_k \cdot \boldsymbol{q}_k\right) d\boldsymbol{x} = 0, \end{aligned}\right\} \tag{17}$$

for all test functions $\boldsymbol{z}_k, \boldsymbol{q}_k \in \mathbb{V}$. The system (17) must be solved for every mode $k \in \mathbb{N}$. For $k = 0$, we obtain a reduced problem: Find $y_0^c, p_0^c \in V$ such that

$$\left.\begin{aligned} &\int_\Omega \left(y_0^c \cdot z_0^c - \nu(\boldsymbol{x})\nabla p_0^c \cdot \nabla z_0^c\right) d\boldsymbol{x} = \int_\Omega y_{d0}^c \cdot z_0^c\, d\boldsymbol{x}, \\ &\int_\Omega \left(\nu(\boldsymbol{x})\nabla y_0^c \cdot \nabla q_0^c + \lambda^{-1} p_0^c \cdot q_0^c\right) d\boldsymbol{x} = 0, \end{aligned}\right\} \tag{18}$$

for all test functions $z_0^c, q_0^c \in V$. The problems (17) and (18) have unique solutions, see (16). In order to solve these problems numerically, the Fourier series are truncated at a finite index N and the unknown Fourier coefficients $\boldsymbol{y}_k = (y_k^c, y_k^s)^T$, $\boldsymbol{p}_k = (p_k^c, p_k^s)^T \in \mathbb{V}$ are approximated by finite element (FE) functions

$$\boldsymbol{y}_{kh} = (y_{kh}^c, y_{kh}^s)^T,\ \boldsymbol{p}_{kh} = (p_{kh}^c, p_{kh}^s)^T \in \mathbb{V}_h = V_h \times V_h \subset \mathbb{V},$$

where $V_h = \mathrm{span}\{\varphi_1, \ldots, \varphi_n\}$ with $\{\varphi_i(\boldsymbol{x}) : i = 1, 2, \ldots, n_h\}$ is a conforming FE space. We denote by h the usual discretization parameter such that $n = n_h = \dim V_h = O(h^{-d})$. In this work, we use continuous, piecewise linear finite elements on a regular triangulation $\mathcal{T}_h$ to construct V_h and its basis (see, e.g., (31; 32; 33; 34)). This leads to the following saddle point system for every single mode $k = 1, 2, \ldots, N$:

$$\begin{pmatrix} M_h & 0 & -K_{h,v} & k\omega M_{h,\sigma} \\ 0 & M_h & -k\omega M_{h,\sigma} & -K_{h,v} \\ -K_{h,v} & -k\omega M_{h,\sigma} & -\lambda^{-1} M_h & 0 \\ k\omega M_{h,\sigma} & -K_{h,v} & 0 & -\lambda^{-1} M_h \end{pmatrix} \begin{pmatrix} \underline{y}^c_k \\ \underline{y}^s_k \\ \underline{p}^c_k \\ \underline{p}^s_k \end{pmatrix} = \begin{pmatrix} \underline{y}^c_{dk} \\ \underline{y}^s_{dk} \\ 0 \\ 0 \end{pmatrix}, \tag{19}$$

which has to be solved with respect to the nodal parameter vectors

$$\underline{y}^c_k = (y^c_{k,i})_{i=1,\ldots,n}, \quad \underline{y}^s_k = (y^s_{k,i})_{i=1,\ldots,n}, \quad \underline{p}^c_k = (p^c_{k,i})_{i=1,\ldots,n}, \quad \underline{p}^s_k = (p^s_{k,i})_{i=1,\ldots,n} \in \mathbb{R}^n$$

of the FE approximations $y^c_{kh}(\boldsymbol{x}) = \sum_{i=1}^n y^c_{k,i}\varphi_i(\boldsymbol{x})$ and $y^s_{kh}(\boldsymbol{x}) = \sum_{i=1}^n y^s_{k,i}\varphi_i(\boldsymbol{x})$. Similarly, $p^c_{kh}(\boldsymbol{x}) = \sum_{i=1}^n p^c_{k,i}\varphi_i(\boldsymbol{x})$ and $p^s_{kh}(\boldsymbol{x}) = \sum_{i=1}^n p^s_{k,i}\varphi_i(\boldsymbol{x})$. The matrices M_h, $M_{h,\sigma}$, and $K_{h,v}$ denote the mass matrix, the weighted mass matrix and the stiffness matrix, respectively. Their entries are defined by the integrals

$$M_h^{ij} = \int_\Omega \varphi_i\varphi_j \, d\boldsymbol{x}, \quad M_{h,\sigma}^{ij} = \int_\Omega \sigma\, \varphi_i\varphi_j \, d\boldsymbol{x}, \quad K_{h,v}^{ij} = \int_\Omega v\, \nabla\varphi_i \cdot \nabla\varphi_j \, d\boldsymbol{x}$$

and the right hand side vectors have the form

$$\underline{y}^c_{dk} = \Big[\int_\Omega y^c_{dk}\varphi_j \, d\boldsymbol{x}\Big]_{j=1,\ldots,n} \quad \text{and} \quad \underline{y}^s_{dk} = \Big[\int_\Omega y^s_{dk}\varphi_j \, d\boldsymbol{x}\Big]_{j=1,\ldots,n}.$$

For $k = 0$, the problem (18) generates a reduced system of linear equations, i.e.,

$$\begin{pmatrix} M_h & -K_{h,v} \\ -K_{h,v} & -\lambda^{-1} M_h \end{pmatrix} \begin{pmatrix} \underline{y}^c_0 \\ \underline{p}^c_0 \end{pmatrix} = \begin{pmatrix} \underline{y}^c_{d0} \\ 0 \end{pmatrix}. \tag{20}$$

Fast and robust solvers for the systems (19) and (20) can be found in (14; 35; 16; 17), which we use in order to obtain the MhFE approximations

$$\left.\begin{aligned} y_{Nh}(\boldsymbol{x}, t) &= y^c_{0h}(\boldsymbol{x}) + \sum_{k=1}^{N} \left(y^c_{kh}(\boldsymbol{x}) \cos(k\omega t) + y^s_{kh}(\boldsymbol{x}) \sin(k\omega t)\right), \\ p_{Nh}(\boldsymbol{x}, t) &= p^c_{0h}(\boldsymbol{x}) + \sum_{k=1}^{N} \left(p^c_{kh}(\boldsymbol{x}) \cos(k\omega t) + p^s_{kh}(\boldsymbol{x}) \sin(k\omega t)\right). \end{aligned}\right\} \tag{21}$$

4. FUNCTIONAL A POSTERIORI ERROR ESTIMATES FOR THE OPTIMALITY SYSTEM

Now we are concerned with *a posteriori* estimates of the difference between the exact solution (y, p) and the respective finite element solution (y_{Nh}, p_{Nh}). First, we present the inf-sup and sup-sup conditions for the bilinear form (16).

Lemma 2. *For all* $y, p \in H^{1,\frac{1}{2}}_{0,per}(Q_T)$*, the space-time bilinear form* $\mathscr{B}(\cdot,\cdot)$ *defined by* (16) *meets the following inf-sup and sup-sup conditions*:

$$\mu_1 \|(y, p)\|_{1,\frac{1}{2}} \leq \sup_{0 \neq (z,q) \in (H^{1,\frac{1}{2}}_{0,per}(Q_T))^2} \frac{\mathscr{B}((y, p), (z, q))}{\|(z, q)\|_{1,\frac{1}{2}}} \leq \mu_2 \|(y, p)\|_{1,\frac{1}{2}}, \tag{22}$$

where $\mu_1 = \left(\min\{\frac{1}{\sqrt{\lambda}}, \underline{\nu}, \underline{\sigma}\} \min\{\sqrt{\lambda}, \frac{1}{\sqrt{\lambda}}\}\right)/\left(\sqrt{1 + 2\max\{\lambda, \frac{1}{\lambda}\}}\right)$ *and* $\mu_2 = \max\{1, \frac{1}{\lambda}, \overline{\nu}, \overline{\sigma}\}$ *are positive constants.*

Proof. Using the triangle and Cauchy-Schwarz inequalities, we obtain

$$\left|\mathscr{B}((y, p), (z, q))\right| = \left| \int_0^T \int_\Omega \Big(y\, z - \nu(\boldsymbol{x}) \nabla p \cdot \nabla z + \sigma(\boldsymbol{x}) \partial_t^{1/2} p\, \partial_t^{1/2} z^{\perp} \right.$$

$$
\begin{aligned}
&\quad + v(\boldsymbol{x})\nabla y \cdot \nabla q + \sigma(\boldsymbol{x})\partial_t^{1/2} y\, \partial_t^{1/2} q^{\perp} + \lambda^{-1} p\, q\Big)\, d\boldsymbol{x}\, dt\Big| \\
&\le \|y\|\|z\| + \overline{v}\,\|\nabla p\|\|\nabla z\| + \overline{\sigma}\,\|\partial_t^{1/2} p\|\,\|\partial_t^{1/2} z\| \\
&\quad + \overline{v}\,\|\nabla y\|\|\nabla q\| + \overline{\sigma}\,\|\partial_t^{1/2} y\|\,\|\partial_t^{1/2} q\| + \lambda^{-1}\,\|p\|\|q\| \\
&\le \mu_2 \|(y,p)\|_{1,\frac{1}{2}} \|(z,q)\|_{1,\frac{1}{2}},
\end{aligned}
$$

where $\mu_2 := \max\{1, \frac{1}{\lambda}, \overline{v}, \overline{\sigma}\}$. Thus, the right hand-side inequality in (22) is proved. In order to prove the left hand-side inequality, we select the test functions

$$
(z,q) = \left(y - \frac{1}{\sqrt{\lambda}} p - \frac{1}{\sqrt{\lambda}} p^{\perp},\, p + \sqrt{\lambda} y - \sqrt{\lambda} y^{\perp} \right).
$$

Using the σ- and v-weighted orthogonality relations (11), we obtain the relations

$$
\begin{aligned}
\mathscr{B}((y,p),(y,p)) &= \|y\|^2 + \lambda^{-1}\|p\|^2, \\
\mathscr{B}((y,p),(-\frac{1}{\sqrt{\lambda}} p, \sqrt{\lambda} y)) &= \frac{1}{\sqrt{\lambda}} \langle v \nabla p, \nabla p \rangle + \sqrt{\lambda} \langle v \nabla y, \nabla y \rangle, \\
\mathscr{B}((y,p),(-\frac{1}{\sqrt{\lambda}} p^{\perp}, -\sqrt{\lambda} y^{\perp})) &= \frac{1}{\sqrt{\lambda}} \langle \sigma \partial_t^{1/2} p, \partial_t^{1/2} p \rangle + \sqrt{\lambda} \langle \sigma \partial_t^{1/2} y, \partial_t^{1/2} y \rangle,
\end{aligned}
$$

which lead to the estimate

$$
\begin{aligned}
&\mathscr{B}\left((y,p), \left(y - \frac{1}{\sqrt{\lambda}} p - \frac{1}{\sqrt{\lambda}} p^{\perp},\, p + \sqrt{\lambda} y - \sqrt{\lambda} y^{\perp} \right)\right) \\
&\quad \ge \min\left\{ \frac{1}{\sqrt{\lambda}}, \underline{v}, \underline{\sigma} \right\} \min\left\{ \sqrt{\lambda}, \frac{1}{\sqrt{\lambda}} \right\} \|(y,p)\|^2_{1,\frac{1}{2}}.
\end{aligned}
$$

Since

$$
\|(z,q)\|^2_{1,\frac{1}{2}} \le \left(1 + 2 \max\left\{ \lambda, \frac{1}{\lambda} \right\} \right) \|(y,p)\|^2_{1,\frac{1}{2}},
$$

we arrive at the estimate

$$\sup_{0\neq(z,q)\in(H^{1,\frac{1}{2}}_{0,per}(Q_T))^2}\frac{\mathscr{B}((y,p),(z,q))}{\|(z,q)\|_{1,\frac{1}{2}}}\geq\frac{\min\{\frac{1}{\sqrt{\lambda}},\underline{\nu},\underline{\sigma}\}\min\{\sqrt{\lambda},\frac{1}{\sqrt{\lambda}}\}\|(y,p)\|^2_{1,\frac{1}{2}}}{\sqrt{1+2\max\{\lambda,\frac{1}{\lambda}\}}\|(y,p)\|_{1,\frac{1}{2}}}$$
$$=\mu_1\,\|(y,p)\|_{1,\frac{1}{2}},$$

where $\mu_1=\left(\min\{\frac{1}{\sqrt{\lambda}},\underline{\nu},\underline{\sigma}\}\min\{\sqrt{\lambda},\frac{1}{\sqrt{\lambda}}\}\right)/\left(\sqrt{1+2\max\{\lambda,\frac{1}{\lambda}\}}\right)$. □

In view of the Friedrichs inequality, the norms $|\cdot|_{1,\frac{1}{2}}$ and $\|\cdot\|_{1,\frac{1}{2}}$ are equivalent. Therefore, Lemma 2 implies the following result:

Lemma 3. *For all $y,p\in H^{1,\frac{1}{2}}_{0,per}(Q_T)$, the bilinear form $\mathscr{B}(\cdot,\cdot)$ satisfies the inf-sup and sup-sup conditions*

$$\tilde{\mu}_1|(y,p)|_{1,\frac{1}{2}}\leq\sup_{0\neq(z,q)\in(H^{1,\frac{1}{2}}_{0,per}(Q_T))^2}\frac{\mathscr{B}((y,p),(z,q))}{|(z,q)|_{1,\frac{1}{2}}}\leq\tilde{\mu}_2|(y,p)|_{1,\frac{1}{2}},\tag{23}$$

where $\tilde{\mu}_1=(\min\{\underline{\nu},\underline{\sigma}\}\min\{\lambda,\frac{1}{\lambda}\})/\sqrt{2}>0$ and $\tilde{\mu}_2=(C_F^2+1)\max\{1,\frac{1}{\lambda},\overline{\nu},\overline{\sigma}\}>0$, and C_F is the Friedrichs constant.

Proof. The right hand-side inequality in (23) results from the triangle and Cauchy-Schwarz inequalities and the Friedrichs inequality (14). Indeed,

$$\left|\mathscr{B}((y,p),(z,q))\right|\leq\max\left\{1,\frac{1}{\lambda},\overline{\nu},\overline{\sigma}\right\}\Big((C_F^2+1)\|\nabla y\|^2+\left\|\partial_t^{1/2}y\right\|^2$$
$$+(C_F^2+1)\|\nabla p\|^2+\left\|\partial_t^{1/2}p\right\|^2\Big)^{1/2}$$
$$\times\Big((C_F^2+1)\|\nabla z\|^2+\left\|\partial_t^{1/2}z\right\|^2$$

$$+ (C_F^2+1)\|\nabla q\|^2 + \left\|\partial_t^{1/2} q\right\|^2\Big)^{1/2}$$

$$\leq \tilde{\mu}_2 |(y,p)|_{1,\frac{1}{2}} |(z,q)|_{1,\frac{1}{2}},$$

where $\tilde{\mu}_2 = (C_F^2+1)\max\{1, \frac{1}{\lambda}, \overline{\nu}, \overline{\sigma}\}$.

The left hand-side inequality in (23) is proved quite similarly to the previous case. We select the test functions

$$(z,q) = \left(-\frac{1}{\sqrt{\lambda}} p - \frac{1}{\sqrt{\lambda}} p^{\perp}, \sqrt{\lambda} y - \sqrt{\lambda} y^{\perp}\right),$$

and use the σ- and ν-weighted orthogonality relations (11). Then, we find that

$$\mathscr{B}\left((y,p), \left(-\frac{1}{\sqrt{\lambda}} p - \frac{1}{\sqrt{\lambda}} p^{\perp}, \sqrt{\lambda} y - \sqrt{\lambda} y^{\perp}\right)\right) \geq \min\{\underline{\nu}, \underline{\sigma}\} \min\left\{\sqrt{\lambda}, \frac{1}{\sqrt{\lambda}}\right\} |(y,p)|^2_{1,\frac{1}{2}}.$$

In view of the estimate

$$|(z,q)|^2_{1,\frac{1}{2}} \leq 2\max\left\{\lambda, \frac{1}{\lambda}\right\} |(y,p)|^2_{1,\frac{1}{2}},$$

we obtain

$$\sup_{0 \neq (z,q) \in (H^{1,\frac{1}{2}}_{0,per}(Q_T))^2} \frac{\mathscr{B}((y,p),(z,q))}{\|(z,q)\|_{1,\frac{1}{2}}} \geq \frac{\min\{\underline{\nu}, \underline{\sigma}\} \min\left\{\sqrt{\lambda}, \frac{1}{\sqrt{\lambda}}\right\} |(y,p)|^2_{1,\frac{1}{2}}}{\sqrt{2}\max\left\{\sqrt{\lambda}, \frac{1}{\sqrt{\lambda}}\right\} |(y,p)|_{1,\frac{1}{2}}}$$

$$= \tilde{\mu}_1 |(y,p)|_{1,\frac{1}{2}},$$

where $\tilde{\mu}_1 = (\min\{\underline{\nu}, \underline{\sigma}\} \min\{\lambda, \frac{1}{\lambda}\})/\sqrt{2}$. This justifies the left hand-side inequality in (23). □

Let (η, ζ) be an approximation of (y,p), which is a bit more regular with respect to the time variable than the exact solution (y,p). Namely, we assume that $\eta, \zeta \in H^{1,1}_{0,per}(Q_T)$ **(this assumption is of course true for the MhFE approximations y_{Nh} and p_{Nh} defined in (21)).** Our

goal is to deduce a computable upper bound of the error $e := (y, p) - (\eta, \zeta)$ in $H^{1,\frac{1}{2}}_{0,per}(Q_T) \times H^{1,\frac{1}{2}}_{0,per}(Q_T)$. **From (15), it follows that the integral identity**

$$\left.\begin{aligned}\int_{Q_T} \Big(&(y-\eta)\, z - \nu(\boldsymbol{x})\nabla(p-\zeta)\cdot\nabla z + \sigma(\boldsymbol{x})\partial_t^{1/2}(p-\zeta)\,\partial_t^{1/2} z^{\perp} \\ &+ \nu(\boldsymbol{x})\nabla(y-\eta)\cdot\nabla q + \sigma(\boldsymbol{x})\partial_t^{1/2}(y-\eta)\,\partial_t^{1/2} q^{\perp} + \lambda^{-1}(p-\zeta)\, q\Big)\, d\boldsymbol{x}\, dt \\ = \int_{Q_T} \Big(&y_d\, z - \eta\, z + \nu(\boldsymbol{x})\nabla\zeta\cdot\nabla z - \sigma(\boldsymbol{x})\partial_t^{1/2}\zeta\,\partial_t^{1/2} z^{\perp} \\ &- \nu(\boldsymbol{x})\nabla\eta\cdot\nabla q - \sigma(\boldsymbol{x})\partial_t^{1/2}\eta\,\partial_t^{1/2} q^{\perp} - \lambda^{-1}\zeta\, q\Big)\, d\boldsymbol{x}\, dt\end{aligned}\right\} \tag{24}$$

holds for all $z, q \in H^{1,\frac{1}{2}}_{0,per}(Q_T)$. The linear functional

$$\begin{aligned}\mathscr{F}_{(\eta,\zeta)}(z, q) = \int_{Q_T} \Big(&y_d\, z - \eta\, z + \nu(\boldsymbol{x})\nabla\zeta\cdot\nabla z - \sigma(\boldsymbol{x})\partial_t^{1/2}\zeta\,\partial_t^{1/2} z^{\perp} \\ &- \nu(\boldsymbol{x})\nabla\eta\cdot\nabla q - \sigma(\boldsymbol{x})\partial_t^{1/2}\eta\,\partial_t^{1/2} q^{\perp} - \lambda^{-1}\zeta\, q\Big)\, d\boldsymbol{x}\, dt,\end{aligned}$$

i.e., the right hand side of (24), is defined on $(z, q) \in H^{1,\frac{1}{2}}_{0,per}(Q_T) \times H^{1,\frac{1}{2}}_{0,per}(Q_T)$. It can be viewed as a quantity measuring the accuracy of (24) for any pair of test functions (z, q). Therefore, getting an upper bound of the error is reduced to the estimation of

$$\sup_{0\neq(z,q)\in(H^{1,\frac{1}{2}}_{0,per}(Q_T))^2} \frac{\mathscr{F}_{(\eta,\zeta)}(z, q)}{\|(z, q)\|_{1,\frac{1}{2}}} \quad \text{or} \quad \sup_{0\neq(z,q)\in(H^{1,\frac{1}{2}}_{0,per}(Q_T))^2} \frac{\mathscr{F}_{(\eta,\zeta)}(z, q)}{|(z, q)|_{1,\frac{1}{2}}}. \tag{25}$$

We rewrite $\mathscr{F}_{(\eta,\zeta)}$ using the identity

$$\langle \sigma\partial_t^{1/2}\eta, \partial_t^{1/2} z^{\perp}\rangle = \langle \sigma\partial_t\eta, z\rangle \quad \forall\, \eta \in H^{1,1}_{0,per}(Q_T)\ \forall\, z \in H^{1,\frac{1}{2}}_{0,per}(Q_T). \tag{26}$$

Also, we use the identities

$$\int_\Omega \operatorname{div}\boldsymbol{\rho}\, z\, d\boldsymbol{x} = -\int_\Omega \boldsymbol{\rho}\cdot\nabla z\, d\boldsymbol{x} \quad \text{and} \quad \int_\Omega \operatorname{div}\boldsymbol{\tau}\, q\, d\boldsymbol{x} = -\int_\Omega \boldsymbol{\tau}\cdot\nabla q\, d\boldsymbol{x},$$

which hold for any $z, q \in H_0^1(\Omega)$ and any

$$\boldsymbol{\tau}, \boldsymbol{\rho} \in H(\mathrm{div}, Q_T) := \{\boldsymbol{\rho} \in [L^2(Q_T)]^d : \mathrm{div}_{\boldsymbol{x}}\, \boldsymbol{\rho}(\cdot, t) \in L^2(\Omega) \text{ for a.e. } t \in (0, T)\}.$$

For ease of notation, the index $\boldsymbol{x}$ in $\mathrm{div}_{\boldsymbol{x}}$ will be henceforth omitted, i.e., $\mathrm{div} = \mathrm{div}_{\boldsymbol{x}}$ denotes the weak spatial divergence. Using the Cauchy-Schwarz inequality yields the estimate

$$\begin{aligned}\mathscr{F}_{(\eta,\zeta)}(z, q) = \int_{Q_T} \Big(& y_d\, z - \eta\, z + \nu(\boldsymbol{x}) \nabla\zeta \cdot \nabla z - \sigma(\boldsymbol{x}) \partial_t \zeta\, z + \mathrm{div}\, \boldsymbol{\rho}\, z + \boldsymbol{\rho} \cdot \nabla z \\ & - \nu(\boldsymbol{x}) \nabla\eta \cdot \nabla q - \sigma(\boldsymbol{x}) \partial_t \eta\, q - \lambda^{-1} \zeta\, q + \mathrm{div}\, \boldsymbol{\tau}\, q + \boldsymbol{\tau} \cdot \nabla q \Big)\, d\boldsymbol{x}\, dt \\ \leq\ & \|\mathscr{R}_1(\eta, \zeta, \boldsymbol{\tau})\| \|q\| + \|\mathscr{R}_2(\eta, \boldsymbol{\tau})\| \|\nabla q\| + \|\mathscr{R}_3(\eta, \zeta, \boldsymbol{\rho})\| \|z\| + \|\mathscr{R}_4(\zeta, \boldsymbol{\rho})\| \|\nabla z\|,\end{aligned}$$

where

$$\left.\begin{aligned} \mathscr{R}_1(\eta, \zeta, \boldsymbol{\tau}) &= \sigma \partial_t \eta + \lambda^{-1} \zeta - \mathrm{div}\, \boldsymbol{\tau}, \quad & \mathscr{R}_2(\eta, \boldsymbol{\tau}) &= \boldsymbol{\tau} - \nu \nabla\eta, \\ \mathscr{R}_3(\eta, \zeta, \boldsymbol{\rho}) &= \sigma \partial_t \zeta + \eta - \mathrm{div}\, \boldsymbol{\rho} - y_d, & \mathscr{R}_4(\zeta, \boldsymbol{\rho}) &= \boldsymbol{\rho} + \nu \nabla\zeta, \end{aligned}\right\} \tag{27}$$

are computable expressions, since all functions are known here. Applying (14), we find that

$$\begin{aligned}\mathscr{F}_{(\eta,\zeta)}(z, q) \leq & \Big(C_F \|\mathscr{R}_1(\eta, \zeta, \boldsymbol{\tau})\| + \|\mathscr{R}_2(\eta, \boldsymbol{\tau})\| \Big) \|\nabla q\| \\ & + \Big(C_F \|\mathscr{R}_3(\eta, \zeta, \boldsymbol{\rho})\| + \|\mathscr{R}_4(\zeta, \boldsymbol{\rho})\| \Big) \|\nabla z\|.\end{aligned}$$

Hence,

$$\begin{aligned}\sup_{0 \neq (z,q) \in (H^{1,\frac{1}{2}}_{0,per}(Q_T))^2} \frac{\mathscr{F}_{(\eta,\zeta)}(z, q)}{|(z, q)|_{1,\frac{1}{2}}} \leq & C_F \|\mathscr{R}_1(\eta, \zeta, \boldsymbol{\tau})\| + \|\mathscr{R}_2(\eta, \boldsymbol{\tau})\| \\ & + C_F \|\mathscr{R}_3(\eta, \zeta, \boldsymbol{\rho})\| + \|\mathscr{R}_4(\zeta, \boldsymbol{\rho})\|\end{aligned}$$

and by the inf-sup condition in (23), we obtain

$$|e|_{1,\frac{1}{2}} \le \frac{1}{\tilde{\mu}_1} \sup_{0\neq(z,q)\in(H^{1,\frac{1}{2}}_{0,per}(Q_T))^2} \frac{\mathscr{B}(e,(z,q))}{|(z,q)|_{1,\frac{1}{2}}} = \frac{1}{\tilde{\mu}_1} \sup_{0\neq(z,q)\in(H^{1,\frac{1}{2}}_{0,per}(Q_T))^2} \frac{\mathscr{F}_{(\eta,\zeta)}(z,q)}{|(z,q)|_{1,\frac{1}{2}}}.$$

Thus, we arrive at the following result:

Theorem 1. *Let* $\eta, \zeta \in H^{1,1}_{0,per}(Q_T)$, $\boldsymbol{\tau}, \boldsymbol{\rho} \in H(\mathrm{div}, Q_T)$, *and the bilinear form* $\mathscr{B}(\cdot,\cdot)$ *defined by* (16) *meets the inf-sup condition* (23). *Then,*

$$\left.\begin{aligned} |e|_{1,\frac{1}{2}} \le \frac{1}{\tilde{\mu}_1}\big(&C_F\,\|\mathscr{R}_1(\eta,\zeta,\boldsymbol{\tau})\| + \|\mathscr{R}_2(\eta,\boldsymbol{\tau})\| \\ &+ C_F\,\|\mathscr{R}_3(\eta,\zeta,\boldsymbol{\rho})\| + \|\mathscr{R}_4(\zeta,\boldsymbol{\rho})\|\big) =: \mathscr{M}^{\oplus}_{|\cdot|}(\eta,\zeta,\boldsymbol{\tau},\boldsymbol{\rho}), \end{aligned}\right\} \tag{28}$$

where $e = (y,p) - (\eta,\zeta) \in (H^{1,\frac{1}{2}}_{0,per}(Q_T))^2$ *and* $\tilde{\mu}_1 = (\min\{\underline{\nu},\underline{\sigma}\}\min\{\lambda,\frac{1}{\lambda}\})/\sqrt{2}$.

Remark 1. For computational reasons, it is useful to reformulate the majorants in such a way that they are given by quadratic functionals, see, e.g., (24). This is done by introducing parameters $\alpha, \beta, \gamma > 0$ and applying Young's inequality. For the error majorant $\mathscr{M}^{\oplus}_{|\cdot|}(\eta,\zeta,\boldsymbol{\tau},\boldsymbol{\rho})$, we have

$$\begin{aligned} \mathscr{M}^{\oplus}_{|\cdot|}(\eta,\zeta,\boldsymbol{\tau},\boldsymbol{\rho})^2 &\le \mathscr{M}^{\oplus}_{|\cdot|}(\alpha,\beta,\gamma;\eta,\zeta,\boldsymbol{\tau},\boldsymbol{\rho})^2 \\ &= \frac{1}{\tilde{\mu}_1^2}\Big(C_F^2(1+\alpha)(1+\beta)\,\|\mathscr{R}_1(\eta,\zeta,\boldsymbol{\tau})\|^2 + \frac{(1+\alpha)(1+\beta)}{\beta}\|\mathscr{R}_2(\eta,\boldsymbol{\tau})\|^2 \\ &\quad + C_F^2\frac{(1+\alpha)(1+\gamma)}{\alpha}\,\|\mathscr{R}_3(\eta,\zeta,\boldsymbol{\rho})\|^2 + \frac{(1+\alpha)(1+\gamma)}{\alpha\gamma}\|\mathscr{R}_4(\zeta,\boldsymbol{\rho})\|^2\Big). \end{aligned}$$

Finally, we note that the inf-sup condition (22) implies an estimate similar to (28) for the error in terms of $\|\cdot\|_{1,\frac{1}{2}}$.

Theorem 2. *Let* $\eta, \zeta \in H^{1,1}_{0,per}(Q_T)$, $\boldsymbol{\tau}, \boldsymbol{\rho} \in H(\mathrm{div}, Q_T)$ *and the bilinear form* $\mathscr{B}(\cdot,\cdot)$ *defined by* (16) *satisfies* (22). *Then,*

$$\left.\begin{aligned} \|e\|_{1,\frac{1}{2}} \leq \frac{1}{\mu_1}\Big(& \|\mathscr{R}_1(\eta,\zeta,\boldsymbol{\tau})\|^2 + \|\mathscr{R}_2(\eta,\boldsymbol{\tau})\|^2 \\ & + \|\mathscr{R}_3(\eta,\zeta,\boldsymbol{\rho})\|^2 + \|\mathscr{R}_4(\zeta,\boldsymbol{\rho})\|^2\Big)^{1/2} =: \mathscr{M}^{\oplus}_{\|\cdot\|}(\eta,\zeta,\boldsymbol{\tau},\boldsymbol{\rho}), \end{aligned}\right\} \tag{29}$$

where e is defined in Theorem 1 *and* $\mu_1 = (\min\{\frac{1}{\sqrt{\lambda}}, \underline{\nu}, \underline{\sigma}\}\min\{\sqrt{\lambda}, \frac{1}{\sqrt{\lambda}}\})/(\sqrt{1+2\max\{\lambda, \frac{1}{\lambda}\}})$.

The multiharmonic approximations

Since the desired state y_d belongs to L^2 it can be represented as a Fourier series. Henceforth, we assume that the approximations η and ζ of the exact state y and the adjoint state p, respectively, are also represented in terms of truncated Fourier series as well as the vector-valued functions $\boldsymbol{\tau}$ and $\boldsymbol{\rho}$, i.e.,

$$\left.\begin{aligned} \eta(\boldsymbol{x},t) &= \eta_0^c(\boldsymbol{x}) + \sum_{k=1}^{N}\left(\eta_k^c(\boldsymbol{x})\cos(k\omega t) + \eta_k^s(\boldsymbol{x})\sin(k\omega t)\right), \\ \boldsymbol{\tau}(\boldsymbol{x},t) &= \boldsymbol{\tau}_0^c(\boldsymbol{x}) + \sum_{k=1}^{N}\left(\boldsymbol{\tau}_k^c(\boldsymbol{x})\cos(k\omega t) + \boldsymbol{\tau}_k^s(\boldsymbol{x})\sin(k\omega t)\right), \end{aligned}\right\} \tag{30}$$

where all the Fourier coefficients belong to the space $L^2(\Omega)$. In this case,

$$\partial_t\eta(\boldsymbol{x},t) = \sum_{k=1}^{N}\left(k\omega\,\eta_k^s(\boldsymbol{x})\cos(k\omega t) - k\omega\,\eta_k^c(\boldsymbol{x})\sin(k\omega t)\right),$$

$$\nabla\eta(\boldsymbol{x},t) = \nabla\eta_0^c(\boldsymbol{x}) + \sum_{k=1}^{N}\left(\nabla\eta_k^c(\boldsymbol{x})\,\cos(k\omega t) + \nabla\eta_k^s(\boldsymbol{x})\,\sin(k\omega t)\right),$$

$$\operatorname{div}\boldsymbol{\tau}(\boldsymbol{x},t)=\operatorname{div}\boldsymbol{\tau}_0^c(\boldsymbol{x})+\sum_{k=1}^{N}\left(\operatorname{div}\boldsymbol{\tau}_k^c(\boldsymbol{x})\,\cos(k\omega t)+\operatorname{div}\boldsymbol{\tau}_k^s(\boldsymbol{x})\,\sin(k\omega t)\right),$$

and the $L^2(Q_T)$-norms of the functions $\mathscr{R}_1$, $\mathscr{R}_2$, $\mathscr{R}_3$ and $\mathscr{R}_4$ defined in (27) can be represented in the form, which exposes each mode separately. More precisely, we have

$$\|\mathscr{R}_1(\eta,\zeta,\boldsymbol{\tau})\|^2=T\|\lambda^{-1}\zeta_0^c-\operatorname{div}\boldsymbol{\tau}_0^c\|_\Omega^2+\frac{T}{2}\sum_{k=1}^{N}\|-k\omega\,\sigma\boldsymbol{\eta}_k^\perp+\lambda^{-1}\boldsymbol{\zeta}_k-\mathbf{div}\,\boldsymbol{\tau}_k\|_\Omega^2,$$

$$\|\mathscr{R}_2(\eta,\boldsymbol{\tau})\|^2=T\|\boldsymbol{\tau}_0^c-\nu\nabla\eta_0^c\|_\Omega^2+\frac{T}{2}\sum_{k=1}^{N}\|\boldsymbol{\tau}_k-\nu\nabla\boldsymbol{\eta}_k\|_\Omega^2,$$

$$\begin{aligned}\|\mathscr{R}_3(\eta,\zeta,\boldsymbol{\rho})\|^2&=T\|\eta_0^c-\operatorname{div}\boldsymbol{\rho}_0^c-y_{d0}^c\|_\Omega^2+\frac{T}{2}\sum_{k=1}^{N}\big(\|k\omega\,\sigma\zeta_k^s+\eta_k^c-\operatorname{div}\boldsymbol{\rho}_k^c-y_{dk}^c\|_\Omega^2\\&\qquad+\|-k\omega\,\sigma\zeta_k^c+\eta_k^s-\operatorname{div}\boldsymbol{\rho}_k^s-y_{dk}^s\|_\Omega^2\big)+\frac{T}{2}\sum_{k=N+1}^{\infty}\big(\|y_{dk}^c\|_\Omega^2+\|y_{dk}^s\|_\Omega^2\big)\\&=T\|\eta_0^c-\operatorname{div}\boldsymbol{\rho}_0^c-y_{d0}^c\|_\Omega^2+\frac{T}{2}\sum_{k=1}^{N}\|-k\omega\,\sigma\boldsymbol{\zeta}_k^\perp+\boldsymbol{\eta}_k-\mathbf{div}\,\boldsymbol{\rho}_k-\boldsymbol{y}_{\boldsymbol{d}k}\|_\Omega^2\\&\qquad+\frac{T}{2}\sum_{k=N+1}^{\infty}\|\boldsymbol{y}_{\boldsymbol{d}k}\|_\Omega^2,\end{aligned}$$

$$\|\mathscr{R}_4(\zeta,\boldsymbol{\rho})\|^2=T\|\boldsymbol{\rho}_0^c+\nu\nabla\zeta_0^c\|_\Omega^2+\frac{T}{2}\sum_{k=1}^{N}\|\boldsymbol{\rho}_k+\nu\nabla\boldsymbol{\zeta}_k\|_\Omega^2,$$

where $\mathbf{div}\,\boldsymbol{\tau}_k=(\operatorname{div}\boldsymbol{\tau}_k^c,\operatorname{div}\boldsymbol{\tau}_k^s)^T$ and $\mathbf{div}\,\boldsymbol{\rho}_k=(\operatorname{div}\boldsymbol{\rho}_k^c,\operatorname{div}\boldsymbol{\rho}_k^s)^T$.

Remark 2. Since y_d is known, we can always compute the remainder term of truncation

$$\mathscr{E}_N:=\frac{T}{2}\sum_{k=N+1}^{\infty}\|\boldsymbol{y}_{\boldsymbol{d}k}\|_\Omega^2=\frac{T}{2}\sum_{k=N+1}^{\infty}\big(\|y_{dk}^c\|_\Omega^2+\|y_{dk}^s\|_\Omega^2\big)\tag{31}$$

with any desired accuracy.

It is important to outline that all the L^2-norms of $\mathscr{R}_1$, $\mathscr{R}_2$, $\mathscr{R}_3$ and $\mathscr{R}_4$ corresponding to every single mode $k = 0, \ldots, N$ are decoupled. It is useful to introduce quantities related to each mode. For $k \geq 1$, we denote them by

$$\begin{aligned}
\mathscr{R}_{1k}(\boldsymbol{\eta}_k, \boldsymbol{\zeta}_k, \boldsymbol{\tau}_k) &:= -k\omega\,\sigma\boldsymbol{\eta}_k^{\perp} + \lambda^{-1}\boldsymbol{\zeta}_k - \mathbf{div}\,\boldsymbol{\tau}_k = (\mathscr{R}_{1k}^{c}(\eta_k^s, \zeta_k^c, \boldsymbol{\tau}_k^c), \mathscr{R}_{1k}^{s}(\eta_k^c, \zeta_k^s, \boldsymbol{\tau}_k^s))^T \\
&= (k\omega\,\sigma\eta_k^s + \lambda^{-1}\zeta_k^c - \operatorname{div}\boldsymbol{\tau}_k^c, -k\omega\,\sigma\eta_k^c + \lambda^{-1}\zeta_k^s - \operatorname{div}\boldsymbol{\tau}_k^s)^T, \\
\mathscr{R}_{2k}(\boldsymbol{\eta}_k, \boldsymbol{\tau}_k) &:= \boldsymbol{\tau}_k - \nu\nabla\boldsymbol{\eta}_k = (\mathscr{R}_{2k}^{c}(\eta_k^c, \boldsymbol{\tau}_k^c), \mathscr{R}_{2k}^{s}(\eta_k^s, \boldsymbol{\tau}_k^s))^T \\
&= (\boldsymbol{\tau}_k^c - \nu\nabla\eta_k^c, \boldsymbol{\tau}_k^s - \nu\nabla\eta_k^s)^T, \\
\mathscr{R}_{3k}(\boldsymbol{\eta}_k, \boldsymbol{\zeta}_k, \boldsymbol{\rho}_k) &:= -k\omega\,\sigma\boldsymbol{\zeta}_k^{\perp} + \boldsymbol{\eta}_k - \mathbf{div}\,\boldsymbol{\rho}_k - \boldsymbol{y_{dk}} \\
&= (\mathscr{R}_{3k}^{c}(\eta_k^c, \zeta_k^s, \boldsymbol{\rho}_k^c), \mathscr{R}_{3k}^{s}(\eta_k^s, \zeta_k^c, \boldsymbol{\rho}_k^s))^T \\
&= (k\omega\,\sigma\zeta_k^s + \eta_k^c - \operatorname{div}\boldsymbol{\rho}_k^c - y_{dk}^c, -k\omega\,\sigma\zeta_k^c + \eta_k^s - \operatorname{div}\boldsymbol{\rho}_k^s - y_{dk}^s)^T,
\end{aligned}$$

and

$$\begin{aligned}
\mathscr{R}_{4k}(\boldsymbol{\zeta}_k, \boldsymbol{\rho}_k) &:= \boldsymbol{\rho}_k + \nu\nabla\boldsymbol{\zeta}_k = (\mathscr{R}_{4k}^{c}(\zeta_k^c, \boldsymbol{\rho}_k^c), \mathscr{R}_{4k}^{s}(\zeta_k^s, \boldsymbol{\rho}_k^s))^T \\
&= (\boldsymbol{\rho}_k^c + \nu\nabla\zeta_k^c, \boldsymbol{\rho}_k^s + \nu\nabla\zeta_k^s)^T.
\end{aligned}$$

For $k = 0$, we have

$$\left.\begin{aligned}
&\mathscr{R}_{10}^{c}(\zeta_0^c, \boldsymbol{\tau}_0^c) := \lambda^{-1}\zeta_0^c - \operatorname{div}\boldsymbol{\tau}_0^c, \qquad \mathscr{R}_{20}^{c}(\eta_0^c, \boldsymbol{\tau}_0^c) := \boldsymbol{\tau}_0^c - \nu\nabla\eta_0^c, \\
&\mathscr{R}_{30}^{c}(\eta_0^c, \boldsymbol{\rho}_0^c) := \eta_0^c - \operatorname{div}\boldsymbol{\rho}_0^c - y_{d0}^c, \; \mathscr{R}_{40}^{c}(\zeta_0^c, \boldsymbol{\rho}_0^c) := \boldsymbol{\rho}_0^c + \nu\nabla\zeta_0^c.
\end{aligned}\right\} \tag{32}$$

Corollary 1. *The error majorants* $\mathscr{M}_{|\cdot|}^{\oplus}(\eta, \zeta, \boldsymbol{\tau}, \boldsymbol{\rho})$ *and* $\mathscr{M}_{\|\cdot\|}^{\oplus}(\eta, \zeta, \boldsymbol{\tau}, \boldsymbol{\rho})$ *defined in* (28) *and* (29), *respectively, can be represented in somewhat new forms that contain quantities associated with*

the modes, namely,

$$\begin{aligned}\mathscr{M}^{\oplus}_{|\cdot|}(\eta,\zeta,\boldsymbol{\tau},\boldsymbol{\rho}) = \frac{1}{\tilde{\mu}_1}\Big(& C_F\left(T\|\mathscr{R}^c_{10}(\zeta^c_0,\boldsymbol{\tau}^c_0)\|^2_\Omega + \frac{T}{2}\sum_{k=1}^N \|\mathscr{R}_{1k}(\boldsymbol{\eta}_k,\boldsymbol{\zeta}_k,\boldsymbol{\tau}_k)\|^2_\Omega\right)^{1/2} \\ & + \left(T\|\mathscr{R}^c_{20}(\eta^c_0,\boldsymbol{\tau}^c_0)\|^2_\Omega + \frac{T}{2}\sum_{k=1}^N \|\mathscr{R}_{2k}(\boldsymbol{\eta}_k,\boldsymbol{\tau}_k)\|^2_\Omega\right)^{1/2} \\ & + C_F\left(T\|\mathscr{R}^c_{30}(\eta^c_0,\boldsymbol{\rho}^c_0)\|^2_\Omega + \frac{T}{2}\sum_{k=1}^N \|\mathscr{R}_{3k}(\boldsymbol{\eta}_k,\boldsymbol{\zeta}_k,\boldsymbol{\rho}_k)\|^2_\Omega + \mathscr{E}_N\right)^{1/2} \\ & + \left(T\|\mathscr{R}^c_{40}(\zeta^c_0,\boldsymbol{\rho}^c_0)\|^2_\Omega + \frac{T}{2}\sum_{k=1}^N \|\mathscr{R}_{4k}(\boldsymbol{\zeta}_k,\boldsymbol{\rho}_k)\|^2_\Omega\right)^{1/2}\Big)\end{aligned}$$

and

$$\begin{aligned}\mathscr{M}^{\oplus}_{\|\cdot\|}(\eta,\zeta,\boldsymbol{\rho},\boldsymbol{\tau}) = \frac{1}{\mu_1}\Big(& T\big(\|\mathscr{R}^c_{10}(\zeta^c_0,\boldsymbol{\tau}^c_0)\|^2_\Omega + \|\mathscr{R}^c_{20}(\eta^c_0,\boldsymbol{\tau}^c_0)\|^2_\Omega + \|\mathscr{R}^c_{30}(\eta^c_0,\boldsymbol{\rho}^c_0)\|^2_\Omega \\ & + \|\mathscr{R}^c_{40}(\zeta^c_0,\boldsymbol{\rho}^c_0)\|^2_\Omega\big) + \frac{T}{2}\sum_{k=1}^N \big(\|\mathscr{R}_{1k}(\boldsymbol{\eta}_k,\boldsymbol{\zeta}_k,\boldsymbol{\tau}_k)\|^2_\Omega + \|\mathscr{R}_{2k}(\boldsymbol{\eta}_k,\boldsymbol{\tau}_k)\|^2_\Omega \\ & + \|\mathscr{R}_{3k}(\boldsymbol{\eta}_k,\boldsymbol{\zeta}_k,\boldsymbol{\rho}_k)\|^2_\Omega + \|\mathscr{R}_{4k}(\boldsymbol{\zeta}_k,\boldsymbol{\rho}_k)\|^2_\Omega\big) + \mathscr{E}_N\Big)^{1/2}.\end{aligned}$$

Remark 3. Let y_d has a multiharmonic representation, i.e.,

$$y_d(\boldsymbol{x},t) = y^c_{d0}(\boldsymbol{x}) + \sum_{k=1}^{N_d}\left(f^c_k(\boldsymbol{x})\cos(k\omega t) + y^s_{dk}(\boldsymbol{x})\sin(k\omega t)\right), \tag{33}$$

where $N_d \in \mathbb{N}$. If $N \geq N_d$, then (η,ζ) is the exact solution of problem (15) and $(\boldsymbol{\tau},\boldsymbol{\rho})$ is the exact flux if and only if the error majorants vanish, i.e.,

$$\mathscr{R}^c_{j0} = 0 \quad \text{and} \quad \mathscr{R}_{jk} = 0 \quad \forall\, k = 1,\ldots,N_d,\ \forall\, j \in \{1,2,3,4\}.$$

Indeed, let the error majorants vanish. Then, $\eta_0^c - \operatorname{div} \boldsymbol{\rho}_0^c = y_{d0}^c$, $\boldsymbol{\rho}_0^c = -\nu\nabla\zeta_0^c$, $\lambda^{-1}\zeta_0^c - \operatorname{div} \boldsymbol{\tau}_0^c = 0$, $\boldsymbol{\tau}_0^c = \nu\nabla\eta_0^c$ and we see that

$$k\omega\,\sigma\eta_k^s + \lambda^{-1}\zeta_k^c - \operatorname{div}\boldsymbol{\tau}_k^c = 0, \quad -k\omega\,\sigma\eta_k^c + \lambda^{-1}\zeta_k^s - \operatorname{div}\boldsymbol{\tau}_k^s = 0,$$

$$k\omega\,\sigma\zeta_k^s + \eta_k^c - \operatorname{div}\boldsymbol{\rho}_k^c = y_{dk}^c, \quad -k\omega\,\sigma\zeta_k^c + \eta_k^s - \operatorname{div}\boldsymbol{\rho}_k^s = y_{dk}^s,$$

$$\boldsymbol{\tau}_k^c = \nu\nabla\eta_k^c, \quad \boldsymbol{\tau}_k^s = \nu\nabla\eta_k^s, \quad \boldsymbol{\rho}_k^c = -\nu\nabla\zeta_k^c, \quad \boldsymbol{\rho}_k^s = -\nu\nabla\zeta_k^s,$$

for all $k = 1, \ldots, N_d$, so that collecting the $N_d + 1$ harmonics leads to multiharmonic representations for η, ζ, $\boldsymbol{\tau}$ and $\boldsymbol{\rho}$ of the form (33) satisfying the equations

$$\sigma\partial_t\eta - \operatorname{div}\boldsymbol{\tau} + \lambda^{-1}\zeta = 0, \quad \boldsymbol{\tau} = \nu\nabla\eta, \qquad \sigma\partial_t\zeta - \operatorname{div}\boldsymbol{\rho} + \eta = y_d, \quad \boldsymbol{\rho} = -\nu\nabla\zeta.$$

This means that $\eta, \zeta \in H^{1,1}_{0,per}(Q_T)$ are solutions of the optimality system. Since they also meet the boundary conditions (due to the assumption), we conclude that $\eta = y$ and $\zeta = p$.

5. FUNCTIONAL A POSTERIORI ESTIMATES FOR COST FUNCTIONALS OF PARABOLIC TIME-PERIODIC OPTIMAL CONTROL PROBLEMS

This section is aimed at deriving guaranteed and computable upper bounds for the cost functional and establishing their sharpness. This is important because, in optimal control, we cannot in general compute the (exact) cost functional since the (exact) state function is unknown. By using *a posteriori* estimates for the state equation we overcome this difficulty. Similar results for elliptic optimal control problems can be found, e.g., in (24; 21). Let $y =$

$y(v)$ be the corresponding state to a control v. The cost functional $\mathcal{J}(y(v), v)$ defined in (1) has the form

$$\mathcal{J}(y(v), v) = T\mathcal{J}_0(y_0^c(v_0^c), v_0^c) + \frac{T}{2}\sum_{k=1}^{\infty}\mathcal{J}_k(\boldsymbol{y}_k(\boldsymbol{v}_k), \boldsymbol{v}_k),$$

where $\mathcal{J}_0(y_0^c(v_0^c), v_0^c) = \frac{1}{2}\|y_0^c - y_{d0}^c\|_\Omega^2 + \frac{\lambda}{2}\|v_0^c\|_\Omega^2$ and

$$\mathcal{J}_k(\boldsymbol{y}_k(\boldsymbol{v}_k), \boldsymbol{v}_k) = \frac{1}{2}\|\boldsymbol{y}_k - \boldsymbol{y}_{dk}\|_\Omega^2 + \frac{\lambda}{2}\|\boldsymbol{v}_k\|_\Omega^2.$$

We wish to deduce majorants for the cost functional $\mathcal{J}(y(u), u)$ of the exact control u and corresponding state $y(u)$ by using some of the results presented in (27), which are obtained for the time-periodic boundary value problem (2). In (27), the following functional *a posteriori* error estimate for problem (2) has been proved:

$$|y(v) - \eta|_{1,\frac{1}{2}} \le \frac{1}{\underline{\mu_1}}\left(C_F\,\|\mathcal{R}_1(\eta, \boldsymbol{\tau}, v)\| + \|\mathcal{R}_2(\eta, \boldsymbol{\tau})\|\right), \tag{34}$$

where $\underline{\mu_1} = \frac{1}{\sqrt{2}}\min\{\underline{\nu}, \underline{\sigma}\}$. It holds for arbitrary functions $\eta \in H^{1,1}_{0,per}(Q_T)$ and $\boldsymbol{\tau} \in H(\mathrm{div}, Q_T)$, where

$$\mathcal{R}_1(\eta, \boldsymbol{\tau}, v) := \sigma\partial_t\eta - \mathrm{div}\,\boldsymbol{\tau} - v, \quad \mathcal{R}_2(\eta, \boldsymbol{\tau}) := \boldsymbol{\tau} - \nu\nabla\eta,$$

and v is a given function in $L^2(Q_T)$. Now, adding and subtracting η in the cost functional $\mathcal{J}(y(v), v)$ as well as applying the triangle and Friedrichs inequalities yields the estimate

$$\mathcal{J}(y(v), v) \le \frac{1}{2}\left(\|\eta - y_d\| + C_F\|\nabla y(v) - \nabla\eta\|\right)^2 + \frac{\lambda}{2}\|v\|^2.$$

Since

$$\|\nabla y(v) - \nabla\eta\|^2 \le |y(v) - \eta|^2_{1,\frac{1}{2}} = \|\nabla y(v) - \nabla\eta\|^2 + \|\partial_t^{1/2} y(v) - \partial_t^{1/2}\eta\|^2,$$

we conclude that

$$\mathcal{J}(y(v), v) \le \frac{1}{2}\left(\|\eta - y_d\| + C_F|y(v) - \eta|_{1,\frac{1}{2}}\right)^2 + \frac{\lambda}{2}\|v\|^2.$$

Together with (34) this leads to the estimate

$$\mathcal{J}(y(v), v) \le \frac{1}{2}\left(\|\eta - y_d\| + \frac{C_F}{\underline{\mu_1}}\|\mathscr{R}_2(\eta, \boldsymbol{\tau})\| + \frac{C_F^2}{\underline{\mu_1}}\|\mathscr{R}_1(\eta, \boldsymbol{\tau}, v)\|\right)^2 + \frac{\lambda}{2}\|v\|^2.$$

By introducing parameters $\alpha, \beta > 0$ and applying Young's inequality, we can reformulate the estimate such that the right-hand side is given by a quadratic functional (the latter functional is more convenient from the computational point of view). We have

$$\mathcal{J}(y(v), v) \le \mathcal{J}^{\oplus}(\alpha, \beta; \eta, \boldsymbol{\tau}, v) \quad \forall\, v \in L^2(Q_T),$$

where

$$\left.\begin{aligned}\mathcal{J}^{\oplus}(\alpha, \beta; \eta, \boldsymbol{\tau}, v) := {} & \frac{1+\alpha}{2}\|\eta - y_d\|^2 + \frac{(1+\alpha)(1+\beta)C_F^2}{2\alpha\underline{\mu_1}^2}\|\mathscr{R}_2(\eta, \boldsymbol{\tau})\|^2 \\ & + \frac{(1+\alpha)(1+\beta)C_F^4}{2\alpha\beta\underline{\mu_1}^2}\|\mathscr{R}_1(\eta, \boldsymbol{\tau}, v)\|^2 + \frac{\lambda}{2}\|v\|^2.\end{aligned}\right\} \tag{35}$$

The majorant (35) provides a guaranteed upper bound of the cost functional, which can be computed for any approximate control and state functions. Moreover, minimization of this

functional with respect to η, $\boldsymbol{\tau}$, v and $\alpha, \beta > 0$ yields the exact value of the cost functional. This important result is summarized in the following theorem:

Theorem 3. *The exact lower bound of the majorant* $\mathcal{J}^{\oplus}$ *defined in* (35) *coincides with the optimal value of the cost functional of problem* (1)–(2), *i.e.*,

$$\inf_{\substack{\eta \in H^{1,1}_{0,per}(Q_T),\, \boldsymbol{\tau} \in H(\mathrm{div}, Q_T) \\ v \in L^2(Q_T),\, \alpha, \beta > 0}} \mathcal{J}^{\oplus}(\alpha, \beta; \eta, \boldsymbol{\tau}, v) = \mathcal{J}(y(u), u). \tag{36}$$

Proof. The infimum of $\mathcal{J}^{\oplus}$ is attained for the optimal control u, the corresponding state function $y(u)$ and the exact flux $(v\nabla y(u))$. In this case, $\mathcal{R}_1$ and $\mathcal{R}_2$ vanish, and for α tending to zero, values of $\mathcal{J}^{\oplus}$ tend to the exact value of the cost functional. □

Corollary 2. *From Theorem* 3, *we obtain the following estimate*:

$$\mathcal{J}(y(u), u) \leq \mathcal{J}^{\oplus}(\alpha, \beta; \eta, \boldsymbol{\tau}, v)$$

$$\forall\, \eta \in H^{1,1}_{0,per}(Q_T),\ \boldsymbol{\tau} \in H(\mathrm{div}, Q_T),\ v \in L^2(Q_T),\ \alpha, \beta > 0. \tag{37}$$

Now, it is easy to derive *a posteriori* estimates for the cost functional in the setting of multiharmonic approximations. Let η be the MhFE approximation y_{Nh} to the state y. Since the control v can be chosen arbitrarily in (35), we choose a MhFE approximation u_{Nh} for it as well. More precisely, we can compute the MhFE approximation u_{Nh} for the control from the MhFE approximation p_{Nh} of the adjoint state, since $u_{Nh} = -\lambda^{-1} p_{Nh}$, by solving the optimality system, from which we obtain y_{Nh} as well. We now apply (37) and select

$\eta = y_{Nh}$ and $v = u_{Nh}$. Next, we need to make a suitable reconstruction of $\boldsymbol{\tau}$, which can be done by different techniques, see, e.g., (21; 26) and the references therein. In the treatment of our approach it is natural to represent $\boldsymbol{\tau}$ in the form of a multiharmonic function $\boldsymbol{\tau}_{Nh}$. Then the majorant

$$\mathcal{J}^{\oplus}(\alpha, \beta; y_{Nh}, \boldsymbol{\tau}_{Nh}, u_{Nh}) = \frac{1+\alpha}{2}\|y_{Nh} - y_d\|^2 + \frac{(1+\alpha)(1+\beta)C_F^2}{2\alpha\underline{\mu_1}^2}\|\mathcal{R}_2(y_{Nh}, \boldsymbol{\tau}_{Nh})\|^2 + \frac{(1+\alpha)(1+\beta)C_F^4}{2\alpha\beta\underline{\mu_1}^2}\|\mathcal{R}_1(y_{Nh}, \boldsymbol{\tau}_{Nh}, u_{Nh})\|^2 + \frac{\lambda}{2}\|u_{Nh}\|^2$$

has a multiharmonic form

$$\begin{aligned}\mathcal{J}^{\oplus}(\alpha, \beta; y_{Nh}, \boldsymbol{\tau}_{Nh}, u_{Nh}) = {} & \frac{1+\alpha}{2}\Big(T\|y_{0h}^c - y_{d0}^c\|_\Omega^2 \\ & + \frac{T}{2}\sum_{k=1}^{N}\left(\|y_{kh}^c - y_{dk}^c\|_\Omega^2 + \|y_{kh}^s - y_{dk}^s\|_\Omega^2\right) + \mathscr{C}_N\Big) \\ & + \frac{(1+\alpha)(1+\beta)C_F^2}{2\alpha\underline{\mu_1}^2}\Big(T\|\mathcal{R}_{20}^c\|_\Omega^2 + \frac{T}{2}\sum_{k=1}^{N}\left(\|\mathcal{R}_{2k}^c\|_\Omega^2 + \|\mathcal{R}_{2k}^s\|_\Omega^2\right)\Big) \\ & + \frac{(1+\alpha)(1+\beta)C_F^4}{2\alpha\beta\underline{\mu_1}^2}\Big(T\|\mathcal{R}_{10}^c\|_\Omega^2 + \frac{T}{2}\sum_{k=1}^{N}\left(\|\mathcal{R}_{1k}^c\|_\Omega^2 + \|\mathcal{R}_{1k}^s\|_\Omega^2\right)\Big) \\ & + \frac{\lambda}{2}\Big(T\|u_{0h}^c\|_\Omega^2 + \frac{T}{2}\sum_{k=1}^{N}\left(\|u_{kh}^c\|_\Omega^2 + \|u_{kh}^s\|_\Omega^2\right)\Big), \end{aligned} \tag{38}$$

where the terms $\mathcal{R}_{10}^c = \operatorname{div}\boldsymbol{\tau}_{0h}^c + u_{0h}^c$, $\mathcal{R}_{20}^c = \boldsymbol{\tau}_{0h}^c - v\nabla y_{0h}^c$,

$$\mathcal{R}_{1k} = k\omega\,\sigma\boldsymbol{y}_{kh}^{\perp} + \mathbf{div}\,\boldsymbol{\tau}_{kh} + \boldsymbol{u}_{kh}$$

$$= (\mathcal{R}_{1k}^c, \mathcal{R}_{1k}^s)^T = (-k\omega\,\sigma y_{kh}^s + \operatorname{div}\boldsymbol{\tau}_{kh}^c + u_{kh}^c, k\omega\,\sigma y_{kh}^c + \operatorname{div}\boldsymbol{\tau}_{kh}^s + u_{kh}^s)^T$$

and

$$\mathcal{R}_{2k} = \boldsymbol{\tau}_{kh} - v\nabla\boldsymbol{y}_{kh} = (\mathcal{R}_{2k}^c, \mathcal{R}_{2k}^s)^T = (\boldsymbol{\tau}_{kh}^c - v\nabla y_{kh}^c, \boldsymbol{\tau}_{kh}^s - v\nabla y_{kh}^s)^T.$$

Note that the remainder term (31) remains the same in (38). Since all the terms corresponding to every single mode k in the majorant $\mathcal{J}^{\oplus}$ are decoupled, we arrive at some majorants $\mathcal{J}_k^{\oplus}$, for which we can, of course, introduce positive parameters α_k and β_k for every single mode k as well. Then the majorant (38) can be written as

$$\mathcal{J}^{\oplus}(\boldsymbol{\alpha}_{N+1}, \boldsymbol{\beta}_N; y_{Nh}, \boldsymbol{\tau}_{Nh}, u_{Nh}) = T\,\mathcal{J}_0^{\oplus}(\alpha_0, \beta_0; y_{0h}^c, \boldsymbol{\tau}_{0h}^c, u_{0h}^c) + \frac{T}{2}\sum_{k=1}^{N}\mathcal{J}_k^{\oplus}(\alpha_k, \beta_k; \boldsymbol{y}_{kh}, \boldsymbol{\tau}_{kh}, \boldsymbol{u}_{kh}) + \frac{1+\alpha_{N+1}}{2}\mathscr{E}_N, \tag{39}$$

where $\boldsymbol{\alpha}_{N+1} = (\alpha_0, \ldots, \alpha_{N+1})^T$, $\boldsymbol{\beta}_N = (\beta_0, \ldots, \beta_N)^T$, and

$$\mathcal{J}_0^{\oplus}(\alpha_0, \beta_0; y_{0h}^c, \boldsymbol{\tau}_{0h}^c, u_{0h}^c) = \frac{1+\alpha_0}{2}\|y_{0h}^c - y_{d0}^c\|_\Omega^2 + \frac{\lambda}{2}\|u_{0h}^c\|_\Omega^2 + \frac{(1+\alpha_0)(1+\beta_0)C_F^2}{2\alpha_0\underline{\mu_1}^2}\|\mathscr{R}_{20}^c\|_\Omega^2 + \frac{(1+\alpha_0)(1+\beta_0)C_F^4}{2\alpha_0\beta_0\underline{\mu_1}^2}\|\mathscr{R}_{10}^c\|_\Omega^2, \tag{40}$$

$$\mathcal{J}_k^{\oplus}(\alpha_k, \beta_k; \boldsymbol{y}_{kh}, \boldsymbol{\tau}_{kh}, \boldsymbol{u}_{kh}) = \frac{1+\alpha_k}{2}\|\boldsymbol{y}_{kh} - \boldsymbol{y}_{dk}\|_\Omega^2 + \frac{\lambda}{2}\|\boldsymbol{u}_{kh}\|_\Omega^2 + \frac{(1+\alpha_k)(1+\beta_k)C_F^2}{2\alpha_k\underline{\mu_1}^2}\|\mathscr{R}_{2k}\|_\Omega^2 + \frac{(1+\alpha_k)(1+\beta_k)C_F^4}{2\alpha_k\beta_k\underline{\mu_1}^2}\|\mathscr{R}_{1k}\|_\Omega^2. \tag{41}$$

Next, we have to reconstruct the fluxes $\boldsymbol{\tau}_{0h}^c$ and $\boldsymbol{\tau}_{kh}$ for all $k = 1, \ldots, N$, which we denote by

$$\boldsymbol{\tau}_{kh} = R_h^{\mathrm{flux}}(\nu\nabla\boldsymbol{y}_{kh}).$$

This can be done by various techniques. In (27), we have used Raviart-Thomas elements of the lowest order (see also (36; 37; 38)), in order to regularize the fluxes by a post-

processing operator, which maps the L^2-functions into $H(\mathrm{div}, \Omega)$. Collecting all the fluxes corresponding to the modes together yields the reconstructed flux

$$\boldsymbol{\tau}_{Nh} = R_h^{\mathrm{flux}}(\nu \nabla y_{Nh}).$$

After performing a simple minimization of the majorant $\mathcal{J}^{\oplus}$ with respect to $\boldsymbol{\alpha}_{N+1}$ and $\boldsymbol{\beta}_N$, we finally arrive at the *a posteriori* estimate

$$\mathcal{J}(y(u), u) \leq \mathcal{J}^{\oplus}(\bar{\boldsymbol{\alpha}}_{N+1}, \bar{\boldsymbol{\beta}}_N; y_{Nh}, \boldsymbol{\tau}_{Nh}, u_{Nh}), \tag{42}$$

where $\bar{\boldsymbol{\alpha}}_{N+1}$ and $\bar{\boldsymbol{\beta}}_N$ denote the optimized positive parameters.

It is worth outlining that the majorant $\mathcal{J}^{\oplus}$ provides a guaranteed upper bound for the cost functional, and, due to Theorem 3, the infimum of the majorant coincides with the optimal value of the cost functional.

Remark 4. In this work, problems with constraints on the control or the state are not considered, but inequality constraints imposed on the Fourier coefficients of the control can easily be included into the MhFE approach, see (13), hence, it may be considered in the *a posteriori* error analysis of parabolic time-periodic optimal control problems as well.

6. NUMERICAL RESULTS

We compute and analyze the efficiency of the above derived *a posteriori* estimates for different cases, namely,

1. the desired state is periodic and analytic in time, but not time-harmonic,

2. the desired state is analytic in time, but not time-periodic, and

3. the desired state is a non-smooth function in space and time.

Note that convergence and other properties of numerical approximations generated by the MhFEM have been studied in (14; 16) for the same three cases. The optimal control problem (1)–(2) is solved on the computational domain $\Omega = (0, 1) \times (0, 1)$ with the Friedrichs constant $C_F = 1/(\sqrt{2}\pi)$ using a uniform simplicial mesh and standard continuous, piecewise linear finite elements. The material coefficients are supposed to be $\sigma = \nu = 1$. In the first two examples, we choose the cost parameter $\lambda = 0.1$, and in the third one, we choose $\lambda = 0.01$. Both choices are common in optimal control, where the parameter λ is rather seen as a weight for the cost of the control than a regularization parameter.

Getting sharp error bounds requires an efficient construction of η, ζ, $\boldsymbol{\tau}$ and $\boldsymbol{\rho}$ in order to compute sharp guaranteed bounds from the majorants. We choose the MhFE approximations (30) for η and $\boldsymbol{\tau}$ as well as for ζ and $\boldsymbol{\rho}$. In order to obtain suitable fluxes $\boldsymbol{\tau}, \boldsymbol{\rho} \in H(\mathrm{div}, Q_T)$, we reconstruct them by the standard lowest-order Raviart-Thomas (RT^0-) extension of normal fluxes. We refer the reader to (27), where the authors have discussed this issue thoroughly.

In order to solve the saddle point systems (19) for $k = 1, \ldots, N$ and (20) for $k = 0$, we use the robust algebraic multilevel preconditioner of Kraus (see (39)) for an inexact realization of the block-diagonal preconditioners

$$\mathscr{P}_k = \begin{pmatrix} D & 0 & 0 & 0 \\ 0 & D & 0 & 0 \\ 0 & 0 & \lambda^{-1}D & 0 \\ 0 & 0 & 0 & \lambda^{-1}D \end{pmatrix}, \tag{43}$$

where $D = \sqrt{\lambda}K_{h,v} + k\omega\sqrt{\lambda}M_{h,\sigma} + M_h$, and

$$\mathscr{P}_0 = \begin{pmatrix} M_h + \sqrt{\lambda}K_{h,v} & 0 \\ 0 & \lambda^{-1}(M_h + \sqrt{\lambda}K_{h,v}) \end{pmatrix}, \tag{44}$$

in the minimal residual method, respectively. The preconditioners (43) and (44) were presented and discussed in (14; 16; 17). The numerical experiments were computed on grids of mesh sizes 16×16 to 256×256. The algorithms were implemented in C++, and all computations were performed on an average class computer with Intel(R) Xeon(R) CPU W3680 @ 3.33 GHz. Note that the presented CPU times t^{sec} in seconds include the computational times for computing the majorants, which are very small in comparison to the computational times of the solver.

In **Example 1**, we set the desired state

$$y_d(\boldsymbol{x}, t) = \frac{e^t \sin(t)}{10}\left(\left(12 + 4\pi^4\right)\sin^2(t) - 6\cos^2(t) - 6\sin(t)\cos(t)\right)\sin(x_1\pi)\sin(x_2\pi),$$

where $T = 2\pi/\omega$ and $\omega = 1$. This function is time-periodic and analytic, but not time-harmonic because of e^t. Hence, the truncated Fourier series approximation of y_d has

to be computed for applying the MhFEM as presented in Section 3. For that, the Fourier coefficients of y_d can be computed analytically, and, then, they are approximated by the FEM. Next the systems (19) and (20) are solved for all $k \in \{0, \ldots, N\}$. We choose the truncation index $N = 8$. Finally, we reconstruct the fluxes by a RT^0-extension and compute the corresponding majorants. The exact state is given by $y(\boldsymbol{x}, t) = e^t \sin(t)^3 \sin(x_1\pi) \sin(x_2\pi)$. In Table 1, we present the CPU times t^{sec}, the majorants

$$\mathscr{M}_{|\cdot|}^{\oplus_0} = \sqrt{2}\Big(C_F\left(\|\mathscr{R}_{10}^c\|_\Omega + \|\mathscr{R}_{30}^c\|_\Omega\right) + \|\mathscr{R}_{20}^c\|_\Omega + \|\mathscr{R}_{40}^c\|_\Omega\Big)$$

and $\mathscr{J}_0^\oplus$ as defined in (40) as well as the corresponding efficiency indices

$$I_{\text{eff}}^{\mathscr{M},0} = \frac{\mathscr{M}_{|\cdot|}^{\oplus_0}}{|(y_0^c, p_0^c) - (\eta_0^c, \zeta_0^c)|_{1,\Omega}}$$

and $I_{\text{eff}}^{\mathscr{J},0} = \mathscr{J}_0^\oplus / \mathscr{J}_0$ obtained on grids of different mesh sizes. Moreover, Table 2 presents the CPU times t^{sec}, the majorants

$$\mathscr{M}_{|\cdot|}^{\oplus_k} = \sqrt{2}\Big(C_F\left(\|\mathscr{R}_{1k}\|_\Omega + \|\mathscr{R}_{3k}\|_\Omega\right) + \|\mathscr{R}_{2k}\|_\Omega + \|\mathscr{R}_{4k}\|_\Omega\Big)$$

and $\mathscr{J}_k^\oplus$ as defined in (41) for $k = 1$ and, finally, the corresponding efficiency indices

$$I_{\text{eff}}^{\mathscr{M},k} = \frac{\mathscr{M}_{|\cdot|}^{\oplus_k}}{|(\boldsymbol{y}_k, \boldsymbol{p}_k) - (\boldsymbol{\eta}_k, \boldsymbol{\zeta}_k)|_{1,\Omega}}$$

and $I_{\text{eff}}^{\mathscr{J},k} = \mathscr{J}_k^\oplus / \mathscr{J}_k$ obtained on grids of different mesh sizes. Similar results are obtained for larger k as well, which is illustrated in Table 3. This table compares the results for the modes $k \in \{0, \ldots, 8\}$ computed on the 256×256-mesh and presents the overall functional error estimates. For that, the remainder term $\mathscr{E}_N$ is precomputed exactly, see Remark 2. It can be

observed in Table 3 that the values of the majorants $\mathscr{M}_{|\cdot|}^{\oplus_k}$ and $\mathscr{J}_k^{\oplus}$ decrease for increasing k, but that the values of the efficiency indices are all about the same, which is a demonstration for the *robustness* of the method with respect to the modes. Note that the overall efficiency index for $N = 6$ is large ($I_{\text{eff}}^{\mathscr{M}} = 3.15$) compared to the efficiency indices corresponding to the single modes. The reason for that is that the remainder term $\mathscr{E}_6 = 640.25$ is still quite large, and hence, more modes are needed. For $N = 8$, the remainder term is $\mathscr{E}_8 = 106.07$, which leads to a much better overall efficiency index ($I_{\text{eff}}^{\mathscr{M}} = 1.69$). The value for the cost functional is however sufficiently accurate with $N = 6$. This example demonstrates that the *a posteriori* error estimates clearly show what amount of modes would be sufficient for representing the solution with a desired accuracy.

In **Example 2**, we set

$$y_d(\boldsymbol{x}, t) = \frac{e^t}{10}\left(-2\cos(t) + (10 + 4\pi^4)\sin(t)\right)\sin(x_1\pi)\sin(x_2\pi),$$

where $T = 2\pi/\omega$ with $\omega = 1$. It is easy to see that this function is time-analytic, but not time-periodic. As in the first example, we compute the MhFE approximation of the desired state and solve the systems (19) and (20) for all $k \in \{0, \ldots, N\}$ with first $N = 6$ and second $N = 8$ being the truncation index. Finally, we compute also the solutions for $N = 10$. The exact state is given by $y(\boldsymbol{x}, t) = e^t \sin(t)\sin(x_1\pi)\sin(x_2\pi)$. The results related to computational expenditures and efficiency indices are quite similar to those for Example 1. Therefore, we present only numerical results in the form similar to Table 3 (see Table 4). In this numerical experiment, we again observe good and satisfying efficiency indices for $\mathscr{M}_{|\cdot|}^{\oplus_k}$. The remainder terms for $N = 6$, $N = 8$ and $N = 10$ are $\mathscr{E}_6 = 44094.84$, $\mathscr{E}_8 = 19869.30$

and $\mathscr{E}_{10} = 10597.20$, respectively. The efficiency index for $\mathscr{M}^{\oplus}_{|\cdot|}$ with $N = 10$ improves a lot compared to the index with $N = 6$. Note that – as in the first example – the efficiency indices for the cost functional are approximately one. This again demonstrates the accuracy of the majorants for the cost functional.

In **Example 3**, we set

$$y_d(\boldsymbol{x}, t) = \chi_{[\frac{1}{4},\frac{3}{4}]}(t)\, \chi_{[\frac{1}{2},1]^2}(\boldsymbol{x}),$$

where χ denotes the characteristic function in space and time. Let $T = 1$, then $\omega = 2\pi$. Again the coefficients of the Fourier expansion associated with y_d can be found analytically. They are

$$y^c_{dk}(\boldsymbol{x}) = \frac{\left(-\sin(\frac{k\pi}{2}) + \sin(\frac{3k\pi}{2})\right)}{k\pi}\, \chi_{[\frac{1}{2},1]^2}(\boldsymbol{x}),$$

and $y^s_{dk}(\boldsymbol{x}) = 0$ for all $k \in \mathbb{N}$. For $k = 0$, $y^c_{d0}(\boldsymbol{x}) = \chi_{[\frac{1}{2},1]^2}(\boldsymbol{x})/2$. Since the exact solution cannot be computed analytically, we compute its MhFE approximation on a finer mesh (512×512-mesh). Since the modes $y^c_{dk}(\boldsymbol{x}) = 0$ for all even $k \in \mathbb{N}$, it suffices to show the results for odd modes as well as for $k = 0$. Table 5 presents the results with truncation index $N = 23$, since the results regarding the efficiency indices are similar for higher modes. The computational times presented include the times for computing the approximations of the exact modes on the finer mesh. The numerical results again show the efficiency of the majorants for both, the discretization error and the cost functional. This is especially observed for the majorant related to the cost functional, which is very close to the exact value (in spite of a really complicated y_d). The majorant $\mathscr{M}^{\oplus}_{|\cdot|}$ exposes an overestimation but

anyway provides realistic estimates of the errors in the state and control functions measured in terms of the combined error norm.

7. CONCLUSIONS AND OUTLOOK

In (27), the authors derived functional-type *a posteriori* error estimates for MhFE approximations to linear parabolic time-periodic boundary value problems. In this work, we extend this technique to the derivation of *a posteriori* error estimates for MhFE solutions of the corresponding distributed optimal control problem which leads to additional challenges in the analysis. The reduced optimality system is nothing but a coupled parabolic time-periodic PDE system for the state and the adjoint state. We are not only interested in computable *a posteriori* error bounds for the state, the adjoint state and the control, but also for the cost functional. In case of linear time-periodic parabolic constraints, the approximation via MhFE functions leads to the decoupling of computations related to different modes. Due to this feature of the MhFEM, we can in principle use different meshes for different modes and independently generate them by adaptive finite element approximations of the respective Fourier coefficients. To assure the quality of approximations constructed in this way, we need fully computable *a posteriori* estimates, which provide guaranteed bounds of global errors and reliable indicators of errors associated with the modes. Then, by prescribing certain bounds, we can finally filter out the Fourier coefficients, which are important for the numerical solution of the problem. This technology will lead to an *adaptive multiharmonic finite element method (AMhFEM)* that will provide complete adaptivity in space and time. The development and the analysis of

such an AMhFEM goes beyond the scope of this paper, but will heavily be based on the results of this paper as described above. It is clear that the functional *a posteriori* estimates derived here for time-harmonic parabolic optimal control problems can also be obtained for distributed time-harmonic eddy current optimal control problems as studied in (18; 19; 20).

ACKNOWLEDGMENTS

The authors gratefully acknowledge the financial support by the Austrian Science Fund (FWF) under the grants NST-0001 and W1214-N15 (project DK4), the Johannes Kepler University of Linz and the Federal State of Upper Austria. Furthermore, the authors would like to express their thanks to the anonymous referees for their helpful hints and suggestions.

REFERENCES

[1] K. Altmann (2013). *Numerische Verfahren der Optimalsteuerung von Magnetfeldern*. PhD thesis, Technical University of Berlin.

[2] K. Altmann, S. Stingelin, and F. Tröltzsch (2014). On some optimal control problems for electrical circuits. *International Journal of Circuit Theory and Applications* 42: 808–830.

[3] B. Houska, F. Logist, J. V. Impe, and M. Diehl (2009). Approximate robust optimization of time-periodic stationary states with application to biochemical processes. In: *Proceedings of the 48th IEEE Conference on Decision and Control*, pp. 6280–6285. Shanghai, China.

[4] P. Neittaanmäki, J. Sprekels, and D. Tiba (2006). *Optimization of Elliptic Systems: Theory and Applications*. Springer.

[5] M. Hinze, R. Pinnau, M. Ulbrich, and S. Ulbrich (2009). *Optimization with PDE constraints*. Mathematical Modelling: Theory and Applications, Vol. 23, Berlin: Springer.

[6] F. Tröltzsch (2010). *Optimal Control of Partial Differential Equations. Theory, Methods and Applications*. Graduate Studies in Mathematics, vol. 112, Providence, RI: AMS.

[7] A. Borzì and V. Schulz (2012). *Computational Optimization of Systems Governed by Partial Differential Equations*. Philadelphia: SIAM.

[8] S. Yamada and K. Bessho (1988). Harmonic field calculation by the combination of finite element analysis and harmonic balance method. *IEEE Trans. Magn.* 24(6): 2588–2590.

[9] F. Bachinger, M. Kaltenbacher, and S. Reitzinger (2002). An efficient solution strategy for the HBFE method. *Proceedings of the IGTE '02 Symposium Graz, Austria* 2:385–389.

[10] F. Bachinger, U. Langer, and J. Schöberl (2005). Numerical analysis of nonlinear multiharmonic eddy current problems. *Numer. Math.* 100:593–616.

[11] F. Bachinger, U. Langer, and J. Schöberl (2006). Efficient solvers for nonlinear time-periodic eddy current problems. *Comput. Vis. Sci.* 9:197–207.

[12] D. M. Copeland and U. Langer (2010). Domain decomposition solvers for nonlinear multiharmonic finite element equations. *J. Numer. Math.* 18:157–175.

[13] M. Kollmann and M. Kolmbauer (2013). A preconditioned MinRes solver for time-periodic parabolic optimal control problems. *Numer. Linear Algebra Appl.* 20:761–784.

[14] M. Kollmann, M. Kolmbauer, U. Langer, M. Wolfmayr, and W. Zulehner (2013). A robust finite element solver for a multiharmonic parabolic optimal control problem. *Comput. Math. Appl.* 65:469–486.

[15] W. Krendl, V. Simoncini, and W. Zulehner (2013). Stability estimates and structural spectral properties of saddle point problems. *Numer. Math.* 124:183–213.

[16] U. Langer and M. Wolfmayr (2013). Multiharmonic finite element analysis of a time-periodic parabolic optimal control problem. *J. Numer. Math.* 21:265–300.

[17] M. Wolfmayr (2014). *Multiharmonic Finite Element Analysis of Parabolic Time-Periodic Simulation and Optimal Control Problems*. PhD thesis, Johannes Kepler University of Linz.

[18] M. Kolmbauer (2012). *The Multiharmonic Finite Element and Boundary Element Method for Simulation and Control of Eddy Current Problems*. PhD thesis, JKU Linz.

[19] M. Kolmbauer and U. Langer (2012). A robust preconditioned MinRes solver for distributed time-periodic eddy current optimal control problems. *SIAM J. Sci. Comput.* 34:B785–B809.

[20] M. Kolmbauer and U. Langer (2013). Efficient solvers for some classes of time-periodic eddy current optimal control problems. *Numerical Solution of Partial Differential Equations: Theory, Algorithms, and Their Applications* 45:203–216.

[21] S. Repin (2008). *A Posteriori Estimates for Partial Differential Equations*. Radon Series on Computational and Applied Mathematics, vol. 4, Berlin: Walter de Gruyter.

[22] S. Repin (2002). Estimates of deviation from exact solutions of initial-boundary value problems for the heat equation. *Rend. Mat. Acc. Lincei* 13:121–133.

[23] A. V. Gaevskaya and S. I. Repin (2005). A posteriori error estimates for approximate solutions of linear parabolic problems. *Differential Equations* 41:970–983.

[24] Gaevskaya, A., Hoppe, R. H. W., Repin, S. (2006). A posteriori estimates for cost functionals of optimal control problems. *Numerical Mathematics and Advanced Applications, Proceedings of the ENUMATH* 2005:308–316.

[25] A. Gaevskaya, R. H. W. Hoppe, and S. Repin (2007). Functional approach to a posteriori error estimation for elliptic optimal control problems with distributed control. *J. Math. Sci.* 144:4535–4547.

[26] O. Mali, P. Neittaanmäki, and S. Repin (2014). *Accuracy Verification Methods. Theory and Algorithms*. Volume 32 of Computational Methods in Applied Sciences. Netherlands: Springer.

[27] U. Langer, S. Repin, and M. Wolfmayr (2015). Functional a posteriori error estimates for parabolic time-periodic boundary value problems. *Comput. Methods Appl. Math.* 15:353–372.

[28] M. Wolfmayr (2016). A note on functional a posteriori estimates for elliptic optimal control problems. *Numer Meth Part Differ Equat*, DOI:10.1002/num.22075.

[29] O. A. Ladyzhenskaya (1973). *The Boundary Value Problems of Mathematical Physics*. Moscow: Nauka (in Russian. Translated in *Appl. Math. Sci.* 49, Springer, 1985).

[30] O. A. Ladyzhenskaya, V. A. Solonnikov, and N. N. Ural'ceva (1968). *Linear and Quasilinear Equations of Parabolic Type*. Providence, RI: AMS.

[31] D. Braess (2005). *Finite Elements: Theory, Fast Solvers, and Applications in Solid Mechanics*. 2nd ed., Cambridge University Press.

[32] P. G. Ciarlet (1978). *The Finite Element Method for Elliptic Problems*, volume 4 of *Studies in Mathematics and its Applications*. Amsterdam: North-Holland. Republished by SIAM in 2002.

[33] M. Jung and U. Langer (2013). *Methode der Finiten Elemente Für Ingenieure: Eine Einführung in die Numerischen Grundlagen und Computersimulation*. 2nd ed., Wiesbaden: Springer.

[34] O. Steinbach (2008). *Numerical Approximation Methods for Elliptic Boundary Value Problems: Finite and Boundary Elements*. New York: Springer.

[35] J. Kraus and M. Wolfmayr (2013). On the robustness and optimality of algebraic multilevel methods for reaction-diffusion type problems. *Comput. Vis. Sci.* 16:15–32.

[36] P. A. Raviart and J. M. Thomas (1977). A mixed finite element method for 2-nd order elliptic problems. *Mathematical Aspects of Finite Element Methods, Lect. Notes Math.* 606:292–315.

[37] F. Brezzi and M. Fortin (1991). *Mixed and Hybrid Finite Element Methods*. Volume 15 of Springer Series in Computational Mathematics. New York: Springer.

[38] J. E. Roberts and J. M. Thomas (1991). Mixed and hybrid methods. *Handbook of numerical analysis* 2:523–639.

[39] J. Kraus (2012). Additive Schur complement approximation and application to multilevel preconditioning. *SIAM J. Sci. Comput.* 34:A2872–A2895.

Table 1: The majorants $\mathscr{M}^{\oplus_0}_{|\cdot|}$ and $\mathscr{J}^{\oplus}_0$, and their efficiency indices (Example 1).

grid	t^{sec}	$\mathscr{M}^{\oplus_0}_{\lvert\cdot\rvert}$	$I^{\mathscr{M},0}_{\text{eff}}$	$\mathscr{J}^{\oplus}_0$	$I^{\mathscr{J},0}_{\text{eff}}$
16×16	0.02	1.75e+01	2.50	1.26e+05	1.01
32×32	0.08	8.20e+00	2.20	1.27e+05	1.00
64×64	0.35	3.92e+00	2.05	1.27e+05	1.00
128×128	1.62	1.91e+00	1.98	1.27e+05	1.00
256×256	7.00	9.44e-01	1.94	1.27e+05	1.00

Table 2: The majorants $\mathscr{M}^{\oplus_1}_{|\cdot|}$ and $\mathscr{J}^{\oplus}_1$, and their efficiency indices (Example 1).

grid	t^{sec}	$\mathscr{M}^{\oplus_1}_{\lvert\cdot\rvert}$	$I^{\mathscr{M},1}_{\text{eff}}$	$\mathscr{J}^{\oplus}_1$	$I^{\mathscr{J},1}_{\text{eff}}$
16×16	0.02	3.40e+01	2.50	4.74e+05	1.00
32×32	0.09	1.59e+01	2.20	4.79e+05	1.00
64×64	0.36	7.63e+00	2.05	4.80e+05	1.00
128×128	1.62	3.72e+00	1.98	4.80e+05	1.00
256×256	6.99	1.84e+00	1.94	4.80e+05	1.00

Table 3: The overall majorants $\mathscr{M}^{\oplus}_{|\cdot|}$ and $\mathscr{J}^{\oplus}$, and their parts computed on a 256×256-mesh (Example 1).

	t^{sec}	$\mathscr{M}^{\oplus}_{|\cdot|}$	$I^{\mathscr{M}}_{\text{eff}}$	$\mathscr{J}^{\oplus}$	$I^{\mathscr{J}}_{\text{eff}}$
$k = 0$	7.00	9.44e-01	1.94	1.27e+05	1.00
$k = 1$	6.99	1.84e+00	1.94	4.80e+05	1.00
$k = 2$	7.02	1.18e+00	1.94	1.99e+05	1.00
$k = 3$	7.17	6.78e-01	1.94	6.74e+04	1.00
$k = 4$	6.95	2.35e-01	1.92	8.42e+03	1.00
$k = 5$	7.01	8.57e-02	1.94	1.13e+03	1.00
$k = 6$	6.70	4.03e-02	1.87	2.29e+02	1.00
$k = 7$	6.77	2.13e-02	2.12	6.37e+01	1.03
$k = 8$	6.87	1.25e-02	2.18	2.19e+01	1.04
overall with $N = 6$	–	1.03e+01	3.15	3.17e+06	1.00
overall with $N = 8$	–	6.13e+00	1.69	3.17e+06	1.00

Table 4: The overall majorants $\mathscr{M}^{\oplus}_{|\cdot|}$ and $\mathscr{J}^{\oplus}$, and their parts computed on a 256×256-mesh (Example 2).

	t^{sec}	$\mathscr{M}^{\oplus}_{|\cdot|}$	$I^{\mathscr{M}}_{\text{eff}}$	$\mathscr{J}^{\oplus}$	$I^{\mathscr{J}}_{\text{eff}}$
$k = 0$	6.86	1.58e+00	1.95	3.56e+05	1.00
$k = 1$	6.89	2.83e+00	1.95	1.14e+06	1.00
$k = 2$	6.79	1.41e+00	1.93	2.85e+05	1.00
$k = 3$	6.86	6.73e-01	1.89	6.69e+04	1.00
$k = 4$	6.76	3.78e-01	1.85	2.19e+04	1.00
$k = 5$	6.93	2.37e-01	1.78	9.05e+03	1.00
$k = 6$	6.83	1.60e-01	1.71	4.38e+03	1.00
$k = 7$	6.73	1.12e-01	1.62	2.37e+03	1.00
$k = 8$	6.99	8.28e-02	1.54	1.40e+03	1.00
$k = 9$	6.83	6.28e-02	1.45	8.74e+02	1.00
$k = 10$	6.87	4.88e-02	1.37	5.75e+02	1.00
overall with $N = 6$	–	6.94e+02	2.56	7.06e+06	1.00
overall with $N = 8$	–	4.75e+02	1.75	7.06e+06	1.00
overall with $N = 10$	–	3.55e+02	1.31	7.06e+06	1.00

Table 5: The majorants and corresponding efficiency indices computed on a 256×256-mesh (Example 3).

	t^{sec}	$\mathcal{M}_{\lvert\cdot\rvert}^{\oplus_k}$	$I_{\text{eff}}^{\mathcal{M}}$	$\mathcal{J}^{\oplus_k}$	$I_{\text{eff}}^{\mathcal{J}}$
$k=0$	38.60	3.96e+02	3.64	8.20e+04	1.32
$k=1$	38.88	4.80e+02	3.73	1.31e+05	1.30
$k=3$	38.82	1.22e+02	2.52	1.35e+04	1.21
$k=5$	38.98	5.58e+01	2.41	4.62e+03	1.14
$k=7$	38.64	3.22e+00	2.45	2.28e+03	1.11
$k=9$	39.06	2.12e+01	2.51	1.35e+03	1.08
$k=11$	38.92	1.50e+01	2.55	8.89e+02	1.07
$k=13$	39.13	1.14e+01	2.62	6.30e+02	1.06
$k=15$	38.59	8.93e+00	2.63	4.68e+02	1.04
$k=17$	38.58	7.36e+00	2.70	3.63e+02	1.04
$k=19$	38.78	6.06e+00	2.69	2.88e+02	1.03
$k=21$	38.72	5.27e+00	2.78	2.36e+02	1.03
$k=23$	38.87	4.47e+00	2.74	1.96e+02	1.02